The Continuous Strength Method for the design of stainless steel hollow section beam-columns

Itsaso Arrayago[a]*, Esther Real[a], Leroy Gardner[b], Enrique Mirambell[a]

[a]*Department of Civil and Environmental Engineering, Universitat Politècnica de Catalunya, Spain*
[b]*Department of Civil Engineering, Imperial College London, United Kingdom*

* Corresponding author: Itsaso Arrayago, Jordi Girona 1-3, Building C1, 08034 Barcelona, Spain, itsaso.arrayago@upc.edu

ABSTRACT

The Continuous Strength Method (CSM) is a deformation based design approach that provides accurate cross-section resistance predictions by making rational allowance for the interaction between cross-section elements, the partial spread of plasticity and the beneficial effects of strain hardening. The CSM can be used in conjunction with advanced analysis for the design of members and frames, but, for hand calculations, member-level stability checks are currently limited to stainless steel hollow section columns failing by flexural buckling. Extension to the design of stainless steel members subjected to combined compression and bending moment is presented in this paper. The analysis is based on numerical results and existing experimental data collected from the literature on stainless steel hollow section members, including members with stocky and slender cross-sections. Comparisons demonstrate that the adoption of the CSM design equations in conjunction with both current and revised interaction factors considerably improves the accuracy of beam-column capacity predictions for members with stocky cross-sections. The analysis on beam-columns with slender sections shows that similar resistance predictions are obtained using Eurocode 3 and the CSM. The reliability of the proposed approach is demonstrated through statistical analyses performed in accordance with EN 1990.

KEYWORDS

beam-column; combined loading; Continuous Strength Method; flexural buckling; local buckling; stainless steel; strain hardening

HIGHLIGHTS

- Extension of the CSM to the stability design of stainless steel beam-columns is presented.
- Accuracy of the CSM for beam-columns is assessed against experimental and FE data.
- The CSM is more accurate than current provisions for members with stocky cross-sections.
- The CSM is consistent with current provisions for members with slender cross-sections.
- The reliability of the proposed design approach is demonstrated by statistical analyses.

1. INTRODUCTION

Corrosion resistance, high ductility and sound mechanical properties are key features that make stainless steels well suited to use in sustainable infrastructure [1-3]. With the high initial cost of the material relative to the more conventionally used carbon steels, appropriate design expressions accounting for the nonlinear stress-strain response and the considerable strain hardening shown by the different stainless steel alloys is important for efficient, economic and sustainable design. During the last decade, the Continuous Strength Method (CSM) has been developed as an alternative approach to the traditional provisions given in the European standards EN 1993-1-4 [4] and EN 1993-1-1 [5], which are based on an elastic-perfectly plastic stress-strain model. The CSM is not based on the classical discrete cross-section classification concept; instead it is underpinned by a base curve that defines the maximum strain ε_{csm} that a cross-section can achieve prior to failure, evaluated in terms of its relative local slenderness, and incorporates material nonlinearity and strain hardening into the design equations. Hence, the CSM has been shown to predict the resistance of metallic cross-sections such as stainless steel [6,7], carbon steel [8,9] and aluminium [10] profiles more accurately than current design provisions.

The CSM has already been included in the latest edition of the European Design Manual for Stainless Steel Structures [11] and the AISC Design Guide 27 [12], and is due to be incorporated into the upcoming versions of prEN 1993-1-4 [13], ASCE 8 [14] and AISC 370 [15]. However, until recently, the CSM only provided analytical design expressions for the calculation of cross-sectional resistances under compression, bending and combined loading conditions; the calculation of member buckling resistances was not covered, other than by second order inelastic analysis [16-18]. Arrayago et al. [19] developed a consistent new CSM approach for the design of stainless steel members under compression, which allows for the influence of material nonlinearity and strain hardening. However, the approach has yet to be applied to members subjected to combined loading.

For stainless steel cross-sections subjected to combined compression plus bending, it has been shown that the adoption of the EN 1993-1-1 [5] interaction curves, but anchored to the CSM, in place of the traditional Eurocode, cross-section capacity end-points, provides improved resistance predictions [20,21]. Regarding the resistance checks for stainless steel members under combined axial compression and bending moment, use of the CSM bending moment resistance as the bending end-point in the design interaction equations for beam-columns with stocky cross-sections has been proposed [22], but no modification was proposed to the flexural buckling resistance (i.e. the compression end-point). This paper presents a design approach for stainless steel beam-columns with hollow sections in which currently available interaction expressions are used in conjunction with CSM resistances for both end-points. Other research accounting for strain hardening effects in stainless steel beam-columns, but based on the Direct Strength Method, can also be found [23].

2. DESIGN OF STAINLESS STEEL MEMBERS

2.1. DESIGN OF STAINLESS STEEL BEAMS ACCORDING TO EN 1993-1-4

Design provisions to determine the capacity of stainless steel beams in the EN 1993-1-4 [4,13] framework are based on the cross-section classification concept. The bending moment resistance $M_{c,Rd}$ of stainless steel cross-sections is calculated using Eq. 1, where M_{Rk} is the characteristic bending moment resistance and γ_{M0} is the partial factor for cross-section resistance. The definition of M_{Rk} depends on the class of the cross-section, being $M_{Rk} = W_{pl}f_y$ for Class 1 or 2 cross-sections, $M_{Rk} = W_{el}f_y$ for Class 3 cross-sections and $M_{Rk} = W_{eff}f_y$ for Class 4 cross-sections, where f_y is the 0.2% proof stress, W_{pl} is the plastic modulus, W_{el} is the elastic modulus and W_{eff} is the effective modulus.

$$M_{c,Rd} = \frac{M_{Rk}}{\gamma_{M0}} \qquad \text{Eq. 1}$$

2.2. DESIGN OF STAINLESS STEEL COLUMNS ACCORDING TO EN 1993-1-4

The traditional design provisions for stainless steel columns given in the current version of EN 1993-1-4 [4] are based on the Ayrton-Perry buckling formulation utilised in EN 1993-1-1 [5] for carbon steel members, where the column strength is determined by reducing the cross-section squash load as per Eq. 2, where A is the cross-section area (or effective area for Class 4 sections), χ is the reduction factor that accounts for flexural buckling effects calculated as function of the member slenderness $\bar{\lambda} = \sqrt{N_{c,Rk}/N_{cr}}$ (in which $N_{c,Rk}$ is the characteristic cross-section squash load and N_{cr} is the elastic flexural buckling load of the column) and γ_{M1} is the partial factor for member instability.

$$N_{b,Rd} = \chi A f_y/\gamma_{M1} \qquad \text{Eq. 2}$$

The reliability of the flexural buckling curves specified in EN 1993-1-4 [4] was recently analysed in [24] and it was concluded that, in some cases, the required partial safety factors exceeded the currently recommended value of 1.10. Thus, lower buckling curves were proposed for stainless steel Square and Rectangular Hollow Section (SHS and RHS) columns with an imperfection factor $\alpha_{EN} = 0.49$ and limiting slenderness values of $\bar{\lambda}_0 = 0.3$ for the austenitic and duplex alloys, and $\bar{\lambda}_0 = 0.2$ for the ferritic alloys. These revised curves have already been adopted in the Design Manual for Stainless Steel Structures [11] and will be included in the next version of prEN 1993-1-4 [13].

2.3. THE CONTINUOUS STRENGTH METHOD FOR THE DESIGN OF STAINLESS STEEL BEAMS

The Continuous Strength Method design equations for predicting the bending moment resistance of stainless steel beams allow for element interaction, the partial spread of plasticity and strain hardening effects; for beams with slender cross-sections the bending capacity is determined directly without requiring the calculation of effective section properties. The CSM bending capacity of stainless steel beams with SHS and RHS sections $M_{c,csm,Rd}$ is calculated from Eq. 3 and Eq. 4 for stocky and slender cross-sections, respectively, where E is the Young's modulus, E_{sh} is the strain hardening slope corresponding to the bi-linear CSM material model [6,7], ε_{csm} is the maximum strain that the cross-section can endure prior to failure, determined from the CSM base curve [6,7], and ε_y is the yield strain, $\varepsilon_y = f_y/E$.

For $\varepsilon_{csm}/\varepsilon_y \geq 1$

$$M_{c,csm,Rd} = \frac{W_{pl} f_y}{\gamma_{M0}} \left[1 + \frac{E_{sh}}{E} \frac{W_{el}}{W_{pl}} \left(\frac{\varepsilon_{csm}}{\varepsilon_y} - 1 \right) - \left(1 - \frac{W_{el}}{W_{pl}} \right) \left(\frac{\varepsilon_{csm}}{\varepsilon_y} \right)^{-2} \right] \qquad \text{Eq. 3}$$

For $\varepsilon_{csm}/\varepsilon_y < 1$

$$M_{c,csm,Rd} = \frac{\varepsilon_{csm}}{\varepsilon_y} \frac{W_{el} f_y}{\gamma_{M0}} \qquad \text{Eq. 4}$$

There has been substantial work on members subjected to pure bending over the last few years, in which the CSM design provisions shown in Eq. 3 and Eq. 4 have been found to provide excellent resistance predictions for stainless steel beams [6,7,25-30]. Studies on RHS beams with stocky cross-sections [6,7,25-29] showed that, on average, the predicted-to-experimental (or numerical) moment ratios increase from 0.74, when the EN 1993-1-4 [4] design equations are used, to 0.88 when the CSM equation (Eq. 3) is adopted [31]. Likewise, and according to the results reported in [30,31], average ratios of bending moment resistance predictions to corresponding test or FE values for stainless steel beams with slender cross-sections are improved from 0.76 to 0.82 when Eq. 4 is adopted instead of the effective width expressions specified in EN 1993-1-4 [4].

2.4. THE CONTINUOUS STRENGTH METHOD FOR THE DESIGN OF STAINLESS STEEL COLUMNS

A new CSM design approach for determining the flexural buckling resistance of stainless steel hollow section columns has been recently developed [19]. This method is based on the traditional Ayrton-Perry formulation but features enhanced CSM cross-section resistances and a generalized imperfection parameter that is a function of cross-section slenderness. From the basic CSM compression and bending moment resistances, $N_{c,csm,Rk}$ and $M_{c,csm,Rk}$, calculated according to the expressions presented in [6,7,11], the flexural buckling resistance of stainless steel members $N_{b,csm,Rd}$ can be calculated using Eq. 5 and following a procedure similar to that prescribed in EN 1993-1-4 [4] and the Design Manual [11] by reducing the basic CSM cross-section capacity in compression $N_{c,csm,Rk}$ with the CSM flexural buckling reduction factor χ_{csm}, which can be calculated from Eq. 6 and Eq. 7 and from the CSM member slenderness $\bar{\lambda}_{csm}$ given by Eq. 8.

$$N_{b,csm,Rd} = \frac{\chi_{csm} N_{c,csm,Rk}}{\gamma_{M1}} \qquad \text{Eq. 5}$$

$$\chi_{csm} = \frac{1}{\phi_{csm} + \sqrt{\phi_{csm}^2 - \bar{\lambda}_{csm}^2}} \qquad \text{Eq. 6}$$

$$\phi_{csm} = 0.5\left[1 + \alpha_{csm}(\bar{\lambda}_{csm} - \bar{\lambda}_0) + \bar{\lambda}_{csm}^2\right] \qquad \text{Eq. 7}$$

$$\bar{\lambda}_{csm} = \sqrt{N_{c,csm,Rk}/N_{cr}} \qquad \text{Eq. 8}$$

The equivalent CSM imperfection factor α_{csm} in Eq. 7 compensates for the detrimental effect of plasticity on member stability, which is not directly captured in the first yield Ayrton-Perry approach, and is given in Eq. 9. In this equation, $\sigma_{c,csm}$ is the CSM cross-section compression failure stress, M_{el} is the elastic bending moment capacity of the cross-section and N_{pl} is the plastic axial resistance.

$$\alpha_{csm} = \alpha_{EN} \frac{e_{0,csm}}{e_{0,el,EN}} \sqrt{\frac{f_y}{\sigma_{c,csm}} \frac{N_{c,csm,Rk} M_{el}}{M_{c,csm,Rk} N_{pl}}} \qquad \text{Eq. 9}$$

The α_{csm} factor is a function of the cross-section slenderness $\bar{\lambda}_p$ through the ratio of member bow imperfection amplitudes $e_{0,csm}/e_{0,el,EN}$ for the CSM and the classical formulation [4,11], as per Eq. 10, adopting the C_5 and C_6 parameters defined in Eq. 11 and Eq. 12, respectively, for stainless steel SHS and RHS members.

$$\frac{e_{0,csm}}{e_{0,el,EN}} = \begin{cases} C_5 - C_6\bar{\lambda}_p & \text{for} \quad \bar{\lambda}_p \leq 0.68 \\ 1 & \text{for} \quad \bar{\lambda}_p > 0.68 \end{cases} \qquad \text{Eq. 10}$$

$$C_5 = 1 + 0.68 C_6 \qquad \text{Eq. 11}$$

$$C_6 = 1.2\left(f_u/f_y\right) \qquad \text{Eq. 12}$$

The approach is based on the revised flexural buckling curves described in the previous section, and thus the values reported in Section 2.2 for $\bar{\lambda}_0$ and α_{EN} are adopted in Eq. 7 and Eq. 9, respectively. The method was shown to provide consistently more accurate column buckling resistance predictions than the current EN 1993-1-4 design rules for all stainless steel families due to consideration given to the interaction between cross-section elements and the allowance made for the partial spread of plasticity and strain hardening [19]. In particular, column resistance predictions in terms of predicted-to-experimental (or numerical) load ratios were found to improve from 0.91 to 0.97 when the CSM design approach for flexural buckling developed in [19] was adopted over the current EN 1993-1-4 design rules for RHS stainless steel columns with stocky cross-sections, while consistent ratios of 0.84 were obtained for columns with slender cross-sections for the two approaches.

2.5. DESIGN OF STAINLESS STEEL MEMBERS SUBJECTED TO COMBINATIONS OF AXIAL LOAD AND BENDING MOMENT

Resistance checks for members under combined axial compression and bending moment, without lateral-torsional buckling, are carried out through interaction equations, such as that given in Eq. 13. In this equation, N_{Ed} and M_{Ed} are the design values of the compression force and bending moment, $N_{b,Rd}$ is the design flexural buckling resistance, $M_{c,Rd}$ is the design bending moment capacity of the cross-section and k is an interaction factor. The accuracy of the interaction equation depends on the values adopted for the flexural buckling and bending moment resistances, which define the end-points of the interaction curve, and on the interaction factor k.

$$\frac{N_{Ed}}{N_{b,Rd}} + k\frac{M_{Ed}}{M_{c,Rd}} \leq 1.0 \qquad \text{Eq. 13}$$

The interaction equation for laterally restrained members under compression and minor axis bending moment according to EN 1993-1-4 [4] is given by Eq. 14, with the interaction factor k_z given in Eq. 15. The term $(N_{b,Rd})_{min}$ in Eq. 14 and Eq. 15 refers to the lowest buckling resistance value for the different buckling modes (flexural buckling about the major axis, flexural buckling about the minor axis, torsional buckling and torsional-flexural buckling) and e_{Nz} is the shift in neutral axis when the cross-section is subjected to uniform compression, which is zero in the case of SHS and RHS. In addition, $\beta_{W,z}$ is a parameter accounting for the cross-section class in bending ($\beta_{W,z} = 1.0$ for Class 1 or 2 cross-sections, $\beta_{W,z} = W_{el,z}/W_{pl,z}$ for Class 3 cross-sections and $\beta_{W,z} = W_{eff,z}/W_{pl,z}$ for Class 4 cross-sections) and $W_{pl,z}$, $W_{el,z}$ and $W_{eff,z}$ are the minor axis plastic, elastic and effective moduli of the cross-section, respectively. In Eq. 15, $\bar{\lambda}_z$ is the column slenderness for minor z-z axis flexural buckling.

$$\frac{N_{Ed}}{(N_{b,Rd})_{min}} + k_z\left(\frac{M_{z,Ed} + N_{Ed}e_{Nz}}{\beta_{W,z}W_{pl,z}f_y/\gamma_{M1}}\right) \leq 1.0 \qquad \text{Eq. 14}$$

$$k_z = 1 + 2(\bar{\lambda}_z - 0.5)\frac{N_{Ed}}{(N_{b,Rd})_{min}} \text{ but } 1.2 \leq k_z \leq 1.2 + 2\frac{N_{Ed}}{(N_{b,Rd})_{min}} \qquad \text{Eq. 15}$$

The interaction factor currently specified in EN 1993-1-4 [4] (Eq. 15) was found to be inaccurate in recent studies [22] and a new expression for the interaction factor k_z was proposed, based on the revised buckling curves given in [24] and the CSM bending moment resistance as end-points. This revised interaction factor is given in Eq. 16, with the D_i coefficients summarized in Table 1 for different families of stainless steel SHS and RHS beam-columns.

$$k_z = 1 + D_1(\bar{\lambda}_z - D_2)\frac{N_{Ed}}{N_{b,Rd,z}} \leq 1 + D_1(D_3 - D_2)\frac{N_{Ed}}{N_{b,Rd,z}} \qquad \text{Eq. 16}$$

In the upcoming prEN 1993-1-4 [13] standard, these new values for the D_i coefficients will be used in conjunction with the general beam-column interaction equations provided in the upcoming version of EN 1993-1-1, prEN 1993-1-1 [32], as recommended in [22,33]; this brings greater consistency between carbon steel and stainless steel design. These interaction equations are given by Eq. 17 and Eq. 18.

$$\frac{N_{Ed}}{\chi_y \, {N_{Rk}}/{\gamma_{M1}}} + k_{yy}\frac{M_{y,Ed} + \Delta M_{y,Ed}}{\chi_{LT}\, {M_{y,Rk}}/{\gamma_{M1}}} + k_{yz}\frac{M_{z,Ed} + \Delta M_{z,Ed}}{{M_{z,Rk}}/{\gamma_{M1}}} \leq 1.0 \qquad \text{Eq. 17}$$

$$\frac{N_{Ed}}{\chi_z \, {N_{Rk}}/{\gamma_{M1}}} + k_{zy}\frac{M_{y,Ed} + \Delta M_{y,Ed}}{\chi_{LT}\, {M_{y,Rk}}/{\gamma_{M1}}} + k_{zz}\frac{M_{z,Ed} + \Delta M_{z,Ed}}{{M_{z,Rk}}/{\gamma_{M1}}} \leq 1.0 \qquad \text{Eq. 18}$$

In these equations, N_{Ed} is the design value of the compression force and $M_{y,Ed}$ and $M_{z,Ed}$ are the design values of the maximum bending moments about the y-y and z-z axes along the member, N_{Rk}, $M_{y,Rk}$ and $M_{z,Rk}$ are the characteristic values of the cross-sectional resistance to compressive axial force and bending moments about the y-y and z-z axes, respectively, and γ_{M1} is the partial factor for the resistance of stainless steel members to instability assessed by member checks, taken as $\gamma_{M1} = 1.10$. $\Delta M_{y,Ed}$ and $\Delta M_{z,Ed}$ are the moments due to the shift of the centroidal axes for Class 4 sections (which are zero for SHS and RHS), χ_y and χ_z are the major and minor axis flexural buckling reduction factors, respectively, and χ_{LT} is the buckling reduction factor for lateral torsional buckling. The interaction factors k_{yy}, k_{yz}, k_{zy} and k_{zz} employed in Eq. 17 and Eq. 18 should be calculated using the expressions given in Table 2 and Table 3 for SHS/RHS with instability governed by buckling about the y-y and z-z axis [13,33]. C_{my} and C_{mz} are the equivalent uniform moment factors, while n_y and n_z are calculated using Eq. 19 and Eq. 20. Note that the k_{yy} and k_{zz} factors reported in Table 2 and Table 3 are the same as those obtained by substituting the D_i coefficients from Table 1 into Eq. 16.

$$n_y = \frac{N_{Ed}}{\chi_y \, {N_{Rk}}/{\gamma_{M1}}} \qquad \text{Eq. 19}$$

$$n_z = \frac{N_{Ed}}{\chi_z \, {N_{Rk}}/{\gamma_{M1}}} \qquad \text{Eq. 20}$$

The beam-columns analysed in the present paper are subjected to bending about the minor axis only (i.e. $M_{y,Ed} = 0$) and failure is therefore governed by bending and buckling about the z-z axis. In this case, the general interaction equations given in Eq. 17 and Eq. 18 can be simplified to Eq. 21, with the interaction factor k_{zz} given in Eq. 22 and Table 1, which is equivalent to that shown in Eq. 16.

$$\frac{N_{Ed}}{\chi_z \, {N_{Rk}}/{\gamma_{M1}}} + k_{zz}\frac{M_{z,Ed} + \Delta M_{z,Ed}}{{M_{z,Rk}}/{\gamma_{M1}}} \leq 1.0 \qquad \text{Eq. 21}$$

$$\text{For } \bar{\lambda}_z < D_3 \qquad k_{zz} = C_{mz}\left[1 + D_1\left(\bar{\lambda}_z - D_2\right)n_z\right] \qquad \text{Eq. 22a}$$

$$\text{For } \bar{\lambda}_z \geq D_3 \qquad k_{zz} = C_{mz}\left[1 + D_1(D_3 - D_2)n_z\right] \qquad \text{Eq. 22b}$$

In this paper, adoption of the CSM flexural buckling and bending moment resistances as the basis (i.e. the end-points) for the design of stainless steel beam-columns is assessed. The analysis is based on experimental results collected from the literature and finite element simulations developed in the current study, both of which are described in Section 3. Beam-columns with stocky cross-sections are analysed in Section 4, while the corresponding analysis for beam-columns with slender cross-sections is presented in Section 5. The reliability of the approach is assessed in Section 6 and the summary of proposals is provided in Section 7. Finally, a worked example illustrating the stability design of a stainless steel beam-column using the Continuous Strength Method is provided in Section 8.

3. EXPERIMENTAL AND NUMERICAL RESISTANCE DATA FOR STAINLESS STEEL MEMBERS UNDER COMBINED LOADING

3.1. COLLECTED EXPERIMENTAL DATA

Experimental results reported in the literature have been collected to complement the developed numerical results [34-40]. All tests were conducted under pin-ended conditions. Test specimens with both fully effective (i.e. non-slender sections with $\bar{\lambda}_p \leq 0.68$) and slender cross-sections (i.e. sections with $\bar{\lambda}_p > 0.68$) have been considered. The key details of the assembled experimental data, including number of tests and ranges of cross-section slenderness and member slenderness, are summarized in Table 4. The cross-section slenderness values were calculated from $\bar{\lambda}_p = \sqrt{f_y/\sigma_{cr,l}}$, in which the elastic critical local buckling stress of the full cross-section $\sigma_{cr,l}$ was estimated using CUFSM [41]. Simple analytical expressions for determining $\sigma_{cr,l}$ of full cross-sections are also available in [42].

3.2. FINITE ELEMENT DATA

3.2.1 Validation of the numerical model

Finite Element (FE) models of stainless steel members under combined loading were developed using the general-purpose software ABAQUS [43] and validated against the experimental results reported in [38]. The mid-surfaces of the cross-sections were modelled using the four-noded shell elements with reduced integration S4R [43], which have been widely used in the modelling of cold-formed stainless steel members [21-23]. After conducting a mesh convergence study, computational efficiency and reliability of results were ensured by adopting a uniform mesh size of 5 mm for the flat parts of the faces of the SHS and RHS members, and four elements for the corner regions. Local and global initial geometric imperfections were introduced into the FE models in the form of elastic buckling mode shapes obtained from prior buckling analyses, following the procedure described in [44], with the imperfection amplitudes measured from the test specimens, as reported in [38]. In this approach, two different buckling analyses are performed for each specimen; in the first, an overall member buckling mode shape was ensured by increasing the shell thickness of the modelled member, while for the second buckling analysis, the thickness was reduced to obtain a local buckling eigenmode. Finally, the result files from both analyses were combined into one single file and appropriate amplitudes were assigned. The measured material properties from the test specimens, as given in [38], were also incorporated into the FE models through nonlinear true stress *vs* true plastic strain relationships, considering separately the flat and corner regions of the cross-sections [45].

Residual stresses in cold-formed specimens primarily correspond to bending residual stresses, since membrane residual stresses are low in magnitude and have been shown to have a negligible influence on structural response [45,46]. According to [46,47], coupons curve longitudinally when cut from cold-formed tubes but return to their original straight shape when they are gripped and loaded in a tensile testing machine. It is assumed that during this straightening process the bending residual stresses are re-introduced into the coupons and consequently, the influence of these residual stresses is implicitly included in the stress-strain curves obtained from tensile tests. Therefore, they do not need to be explicitly incorporated into the FE models. To replicate the pin-ended boundary conditions of the tests, the nodes at the ends of the members were kinematically coupled and connected to two reference points, to which the relevant boundary conditions were applied. To model combined loading conditions, reference points were defined with appropriate eccentricities and the load was introduced as an imposed displacement at the upper reference point. The geometrically and materially nonlinear FE analyses were solved using the modified Riks method [43].

The accuracy of the developed beam-column FE models is demonstrated in Table 5, where the ratios of the numerical-to-experimental ultimate loads ($N_{u,FE}/N_{u,exp}$) and corresponding lateral deflections ($\delta_{u,FE}/\delta_{u,exp}$) are reported, showing good agreement between the test and FE failure loads with the mean value of $N_{u,FE}/N_{u,exp}$ equal to 1.02 and the coefficient of variation (COV) equal to 0.017. Comparisons were also made between the experimental and numerical load-deformation curves and failure modes, typical examples of which are presented in Figure 1; the load-deformation histories and failure modes from the tests are seen to be accurately replicated by the FE simulations. Overall, it may be concluded that the developed FE models are capable of accurately predicting the behaviour of stainless steel beam-columns and are suitable for generating parametric results.

3.2.2 Parametric study

The parametric study featured SHS and RHS austenitic, ferritic and duplex stainless steel members with pin-ended conditions and both stocky and slender cross-sections under combined loading. For each stainless steel family (austenitic, ferritic and duplex alloys), the parametric study included SHS and RHS cross-sections with overall height and width dimensions ranging between 60-180 mm and thicknesses varying between 3-6 mm. Member lengths were chosen to give member slenderness $\bar{\lambda}_{\mathrm{csm}}$ values between 0.4-2.5 and load eccentricities *e* were defined such that *e/B* ranged between 0.1-1.5, where *B* is the width of the cross-section. A total of 180 beam-columns with stocky sections and 84 with slender cross-section were simulated for each material type. The material stress-strain response of each stainless steel family was based on the standardized material parameters reported in [24] for the flat and corner regions of the SHS/RHS, as summarized in Table 6, which were based on experimentally measured properties and therefore already incorporate the effect of bending residual stresses [46,47], and the material model defined in [48]. In Table 6, E is the Young's modulus, f_{y} is the yield stress, f_{u} is the ultimate tensile strength, ε_{u} is the corresponding ultimate strain and *n* and *m* are the strain hardening exponents. Initial global and local imperfections were introduced following the procedure described in Section 3.2.1, with amplitudes equal to L/1500 for the global imperfections, and amplitudes predicted using the modified Dawson and Walker model proposed in [49] for the local imperfections. All the analyses presented in this paper are based on the weighted average material properties of the cross-sections, based on the areas corresponding to the flat and corner regions of the SHS/RHS [11].

4. CSM DESIGN OF STAINLESS STEEL MEMBERS WITH STOCKY CROSS-SECTIONS UNDER COMBINED LOADING

4.1. ASSESSMENT OF EXISTING INTERACTION FACTORS

An assessment of the proposed CSM approach for the design of stainless steel SHS and RHS beam-columns is carried out by comparing the predicted resistances for the different design approaches described below with the experimental and numerical results introduced in Section 3. The assessment is presented separately for members with stocky and slender cross-sections to evaluate the beneficial influence of strain hardening in member design and to assess the accuracy of the CSM strength curve for local buckling, respectively. This section covers members with cross-section slenderness values $\bar{\lambda}_{\mathrm{p}} \leq 0.68$ (i.e. stocky cross-sections), while the next section addresses members with cross-section slenderness values $\bar{\lambda}_{\mathrm{p}} > 0.68$ (i.e. slender cross-sections).

The design approach provided in the current EN 1993-1-4 [4] standard, which is denoted as Design Approach 0 and is based on the interaction equation shown in Eq. 14, with the interaction factor defined in Eq. 15, and the EN 1993-1-4 [4] end-points (pure flexural buckling and pure bending moment resistances) $\mathrm{N_{b,Rk}}$ and $\mathrm{M_{c,Rk}}$, has been adopted as a reference in this study (see Figure 2). Three additional design approaches have been considered using the interaction equation given in Eq. 21, in conjunction with the interaction factor provided in Table 3 or Eq. 22, to illustrate the importance of the adopted end-points, as shown in Figure 2: Design Approach 1 is based on the EN 1993-1-4 [4] end-points ($\mathrm{N_{b,Rk}}$ and $\mathrm{M_{c,Rk}}$), Design Approach 2 combines the classical flexural buckling resistance given in [4] with the CSM bending moment resistance ($N_{b,Rk}$ and $M_{c,csm,Rk}$) and Design Approach 3 incorporates the CSM-based end-points for both flexural buckling and bending moment resistances ($N_{b,csm,Rk}$ and $M_{c,csm,Rk}$). Note that the interaction curve corresponding to Design Approach 0 is not anchored to the bending resistance end-point $M_{c,Rk}$, as shown in Figure 2, owing to the lower limitation of 1.2 in the interaction factor given in Eq. 15. An additional approach – Design Approach 4 – that uses a new interaction factor calibrated in the next section of this paper, with the CSM-based end-points ($N_{b,csm,Rk}$ and $M_{c,csm,Rk}$), is also considered. Table 7 provides a summary of the five Design Approaches considered in the analysis of beam-columns with stocky cross-section, indicating the flexural buckling resistance, bending moment resistance, interaction equation and interaction factors considered in each case. For the analysis of the results, an angle parameter θ is introduced in Eq. 23 and Figure 3 to describe the combination of axial load and bending moment, in which N_{pred} and M_{pred} are the predicted compression and bending moment resistances, N_u and M_u are the ultimate numerical (or experimental) compression and bending moment capacities and $N_{b,R}$ and $M_{c,R}$ represent the pure flexural buckling and pure bending moment resistances. In this paper, the CSM end-points have been adopted for the calculation of the angle parameter θ, as shown in Eq. 23. Note that $\theta = 0°$ represents pure bending loading conditions, while $\theta = 90°$ corresponds to pure compression.

$$\theta = \tan^{-1}\left[\frac{N_{pred}/N_{b,csm,Rk}}{M_{pred}/M_{c,sm,Rk}}\right] = \tan^{-1}\left[\frac{N_u/N_{b,csm,Rk}}{M_u/M_{c,csm,Rk}}\right] \quad \text{Eq. 23}$$

The results for the stainless steel beam-columns with stocky cross-sections are presented separately for values of the angle parameter θ lower and higher than 45° in Table 8 to illustrate loading scenarios governed by bending, with $0° \leq \theta < 45°$, and by compression, with $45° \leq \theta \leq 90°$, as well as for all loading scenarios ($0° \leq \theta \leq 90°$). Table 8 presents the mean values and coefficients of variation (COV) of the predicted-to-ultimate experimental or numerical axial load ratios for the different design approaches and stainless steel families considered. Since proportional loading is applied to all experimental and FE beam-columns considered in this study, calculating the predicted-to-ultimate axial load ratios N_{pred}/N_u is equivalent to the combined compression plus bending predicted-to-ultimate capacity ratios. From the mean values and coefficients of variation of the N_{pred}/N_u ratios reported in Table 8 for $0° \leq \theta < 45°$, similar conclusions can be drawn for the three stainless steel families – the most accurate beam-column capacity predictions are obtained when both the flexural buckling and bending moment resistances are calculated using the CSM, i.e. using $N_{b,csm,Rk}$ and $M_{c,csm,Rk}$ as the end-points in Design Approach 3. The most substantial improvements are observed for the austenitic alloys (which exhibit the most pronounced strain hardening among the three stainless steel families considered) and a consistent level of accuracy is achieved for all three materials.

When all specimens are analysed in Table 8, improvements in the prediction of beam-column strengths can be observed from Design Approach 1 to Design Approach 2 and from Design Approach 2 to Design Approach 3. However, for low values of the angle parameter ($0° \leq \theta < 45°$), improvements mainly occur from Design Approach 1 to Design Approach 2 when the end-point corresponding to the bending moment resistance is modified, since these specimens are subjected primarily to bending (see Table 8 for $0° \leq \theta < 45°$). According to the results reported in Table 8, for specimens loaded under predominantly compressive loading (with high values of the angle parameter θ, i.e. $45° \leq \theta \leq 90°$), improvements are observed when the CSM is used for both the bending moment and the flexural buckling resistance predictions. This is because the second term accounting for bending effects in the interaction equation (see Eq. 14 or Eq. 21) has a stronger impact on the final interaction check as it incorporates the interaction factor k which typically assumes a value greater than unity. Finally, it is worth noting that while the results reported for austenitic stainless steel for the Design Approaches 0 and 1 are similar, improvements in the predicted capacities can be observed for the ferritic and duplex families when the interaction factor given in Eq. 16 or Eq. 22 is adopted. This can be explained by the D_i coefficients reported in Table 1, which lead to similar interaction factors for Design Approaches 0 and 1 for austenitic stainless steel beam-columns ($D_1 = 2.0$ and $D_2 = 0.50$ vs. $D_1 = 2.0$ and $D_2 = 0.30$), but rather different factors for the remaining stainless steel families.

Figure 4 to 6 present comparisons of the predicted-to-ultimate compression ratios corresponding to the different design approaches and stainless steel families considered. The results are plotted against the angle parameter θ for the austenitic, ferritic and duplex stainless steel beam-columns with stocky cross-sections in Figure 4, Figure 5 and Figure 6, respectively. For comparison purposes, results corresponding to the end-points i.e. pure bending ($\theta = 0°$) and pure compression ($\theta = 90°$) reported in the literature [19,25-29] are also included, although the analysis is focussed on members subjected to combined loading conditions. These figures illustrate the improvement obtained in the prediction of the resistance of cold-formed stainless steel hollow section beam-columns when more accurate analytical models are considered for the calculation of the end-points defining the axial compression-bending moment interaction diagrams: the lowest N_{pred}/N_u ratios are observed for Design Approaches 0 and 1 for the three material families, since these approaches do not incorporate strain hardening effects into the calculation of the end-points. It can be also observed that the results for Design Approaches 2 and 3 are very similar for specimens under combined loading with low θ values (i.e. loading governed by bending moment), which indicates that improvement to the prediction of flexural buckling resistance does not have a significant influence on the resistance prediction of beam-columns with high bending moment-to-compression ratios. However, for high θ values (i.e. members loaded predominantly in compression), the improvement introduced by the new CSM approach for stainless steel columns is considerable.

It is worth noting that Figures 4 to 6 include a few cases in which Design Approach 2 provides higher N_{pred}/N_u ratios than Design Approach 3, which might seem counterintuitive. The explanation for this can be found in the definition of the interaction factors k given in Eq. 16 and Eq. 22, and in Table 2 and Table 3, which are dependent on both the member slenderness $\bar{\lambda}$ (or $\bar{\lambda}_{csm}$) and the flexural buckling resistance $N_{b,Rk}$ (or $N_{b,csm,Rk}$). The coefficients D_1, D_2 and D_3 were originally calibrated for member slenderness $\bar{\lambda}$ values calculated according to EN 1993-1-4 [4] and the flexural buckling resistances $N_{b,Rk}$ proposed in [24]. When adopting the new parameters – $\bar{\lambda}_{csm}$ and $N_{b,csm,Rk}$ based on CSM resistances – it is observed that in general, the considered member slenderness has a stronger influence on the calculation of the interaction factor k, which indicates that for the same specimen, the interaction factor would be higher for the CSM than for the current design approach, resulting in a lower member capacity prediction. Thus, a recalibration of the D_i coefficients based on the CSM resistances is required, which is addressed in the following sub-section.

4.2. DEVELOPMENT OF NEW INTERACTION FACTORS

Although the adoption of the CSM design equations for stainless steel beam-columns in conjunction with the original D_1, D_2 and D_3 coefficients [22] leads to an overall improvement in the predicted member capacities, the accuracy of the method can be further improved by recalibrating the D_i coefficients to account for the different CSM member slendernesses and column buckling resistances. The new interaction factor $k_{zz,csm}$ is defined following the same structure to that given in Eq. 22, but with modified coefficients $D_{1,csm}$, $D_{2,csm}$ and $D_{3,csm}$, as per Eq. 24.

$$\text{For } \bar{\lambda}_{z,csm} < D_{3,csm} \qquad k_{zz,csm} = C_{mz}\left[1 + D_{1,csm}\left(\bar{\lambda}_{z,csm} - D_{2,csm}\right)n_{z,csm}\right] \qquad \text{Eq. 24a}$$

$$\text{For } \bar{\lambda}_{z,csm} \geq D_{3,csm} \qquad k_{zz,csm} = C_{mz}\left[1 + D_{1,csm}\left(D_{3,csm} - D_{2,csm}\right)n_{z,csm}\right] \qquad \text{Eq. 24b}$$

The new $D_{i,csm}$ coefficients are based on the D_i values originally calibrated by Zhao et al. [22], but incorporate a correction factor γ (given by Eq. 25), that depends on the cross-sectional slenderness through the CSM cross-sectional design stress in compression $\sigma_{c,csm}$ used in column design (see section 2.4), and are defined in Eq. 26 to Eq. 28. The purpose of introducing this correction factor γ is to compensate for the increase in the interaction factor k when the new CSM parameters $\bar{\lambda}_{csm}$ and $N_{b,csm,Rk}$ are adopted, as highlighted in Section 4.1, and to achieve the same flexural buckling and bending moment interaction levels as for the current design approach. Put simply, the objective of the new $D_{i,csm}$ coefficients is to ensure that the k_{zz} and $k_{zz,csm}$ interaction factors are as similar as possible. Note that the new $D_{i,csm}$ coefficients differ to the greatest extent from the original D_i coefficients for the stockiest cross-sections (i.e. low $\bar{\lambda}_p$ or high $\sigma_{c,csm}$ values) and tend to the original D_i values as the cross-section slenderness tends to the limiting value of $\bar{\lambda}_p = 0.68$, which is the CSM slenderness limit between fully effective and slender cross-sections. At $\bar{\lambda}_p = 0.68$, the $D_{i,csm}$ and original D_i values are equal, since $f_y = \sigma_{c,csm}$ and $\gamma = 1.0$.

$$\gamma = \sqrt{f_y/\sigma_{c,csm}} \qquad \text{Eq. 25}$$

$$D_{1,csm} = \gamma D_1 \qquad \text{Eq. 26}$$

$$D_{2,csm} = D_2/\gamma \qquad \text{Eq. 27}$$

$$D_{3,csm} = D_3/\gamma \qquad \text{Eq. 28}$$

A comparison of the interaction factors ($k_{zz,EN}$ and $k_{zz,csm}$) obtained using the original D_i and the new $D_{i,csm}$ coefficients is presented in Figure 7. This figure depicts the ratios of the EN-to-CSM interaction factors for the current definition of the interaction factor (Eq. 22, with empty markers) and the revised interaction factor (Eq. 24, with solid markers) for the three stainless steel families considered, for varying local slenderness values $\bar{\lambda}_p$. The reference interaction factor $k_{zz,EN}$ corresponds to the interaction factors given in Table 3 and Eq. 22, calculated based on the EN 1993-1-4 [4] end-points $N_{b,Rk}$ and $M_{c,Rk}$, while $k_{zz,csm}$ factors have been calculated using the CSM end-points $N_{b,csm,Rk}$ and $M_{c,csm,Rk}$. Figure 7 clearly illustrates that without the correction factor γ, the interaction factors calculated with the CSM end-points and Table 3 are considerably higher than the reference interaction factors $k_{zz,EN}$, which leads to lower member capacity predictions, as highlighted in Section 4.1. On the other hand, when the $k_{zz,csm}$ interaction factors are determined with the new $D_{i,csm}$ coefficients and the CSM end-points, the resulting interaction factors are very close to the reference values $k_{zz,EN}$.

Results corresponding to the application of the new interaction factor $k_{zz,csm}$ are presented in Table 8 as Design Approach 4; the same experimental and numerical database has been employed in the assessment as used for Design Approaches 0 to 3. From the results, it can be seen that the adoption of the new interaction factor $k_{zz,csm}$, defined in Eq. 24, improves the resistance predictions obtained using the Design Approach 3 and provides a more uniform level of accuracy for all materials and loading types. Similar conclusions can be drawn from the predicted-to-ultimate compression ratios reported in Figures 4 to 6 for austenitic, ferritic and duplex stainless steel beam-columns.

5. CSM DESIGN OF STAINLESS STEEL MEMBERS WITH SLENDER CROSS-SECTIONS UNDER COMBINED LOADING

5.1. ASSESSMENT OF EXISTING INTERACTION FACTORS

The assessment of the CSM approach for the design of stainless steel beam-columns with slender cross-sections (i.e. $\bar{\lambda}_p > 0.68$) is presented in this section. As in the previous section, resistance predictions corresponding to the design approaches of Eurocode 3 are calculated and compared with equivalent results based on CSM provisions, for which five design approaches have been defined. Note that design approaches considered in the analysis of the beam-columns with slender cross-sections are slightly different to those defined in Section 4. Table 9 provides a summary of the different Design Approaches investigated in this section, which are also illustrated in Figure 8. In this section, Design Approaches A and B correspond to the general interaction equation given in Eq. 21, with the current interaction factor k_{zz} as defined in Eq. 22, but while Design Approach A is based on the effective end-points calculated following the Effective Width Method provided in EN 1993-1-4 [4] ($N_{b,eff,Rk}$ and $M_{c,eff,Rk}$), Design Approach B adopts the reduced CSM flexural buckling and bending moment resistances for slender sections ($N_{b,eff,csm,Rk}$ and $M_{c,eff,csm,Rk}$), as defined in [19] and [30], respectively. Note that while Design Approach A is equivalent to the Design Approach 1 investigated in Section 4, Design Approach B can be considered equivalent to Design Approach 3. As in Section 4, a reference design approach (Design Approach 0) has been defined for comparison purposes, which is based on the interaction equation shown in Eq. 14 with the interaction factor defined in Eq. 15 and the EN 1993-1-4 [4] end-points $N_{b,eff,Rk}$ and $M_{c,eff,Rk}$.

Ultimate loads calculated following Design Approaches A and B are compared with the corresponding experimental and FE resistances in Table 10, where mean values and coefficients of variation (COV) of the predicted-to-experimental (or FE) load ratios are reported for the different loading types considered (i.e. loading scenarios dominated by bending, with $0° \leq \theta < 45°$, or compression, with $45° \leq \theta \leq 90°$, and all loading conditions, $0° \leq \theta \leq 90°$). The results indicate that both design approaches yield very similar results, although Design Approach B, based on CSM end-points, provides marginally more accurate resistance predictions for stainless steel SHS and RHS beam-columns with slender cross-sections. In addition, this approach is simpler to use, since no effective width calculations are required. These results are consistent with the conclusions reported by the authors in [19] for stainless steel SHS and RHS columns with slender cross-sections. Regarding the reference Design Approach 0, results in Table 10 indicate that, following the observations made for beam-columns with stocky cross-sections, member capacity predictions for Design Approaches 0 and A are similar for austenitic stainless steel, but more conservative for the current design approach provided in [4] (Design Approach 0) for the duplex and ferritic stainless steels. As for Section 4, this is because the D_i coefficients reported in Table 1 for austenitic stainless steel beam-columns result in similar interaction factors for Design Approaches 0 and A, but this is not the case for the ferritic and duplex stainless steels.

Similar results are also shown in Figures 9 to 11, where the predicted-to-experimental (or FE) load ratios are plotted against the angle parameter θ for austenitic, ferritic and duplex stainless steel beam-columns with slender cross-sections. These figures also show results corresponding to pure bending and pure compression (i.e. the end-points), which were obtained from previous studies by the authors [19,27-29], although the analysis is focussed on members subjected to combined loading conditions. The accuracy observed in the predictions of the resistance of stainless steel beam-columns with slender SHS and RHS profiles is markedly lower than that reported for equivalent beam-columns with stocky cross-sections in Section 4. With the aim of providing uniform accuracy levels across the full range of cross-section slenderness, recalibration of the D_i coefficients for beam-columns with slender cross-sections is presented in the following sub-section.

5.2. DEVELOPMENT OF NEW INTERACTION FACTORS

New interaction factors for stainless steel SHS and RHS beam-columns with slender cross-sections are derived in this section. The new interaction factors are applicable for use with both the Eurocode 3 (see Eq. 29) and CSM (see Eq. 30) end-points, which are similar for slender SHS and RHS profiles.

For $\bar{\lambda}_z < D_3^*$ $$k_{zz}^* = C_{mz}\left[1 + D_1^*\left(\bar{\lambda}_z - D_2^*\right)n_z\right] \quad \text{Eq. 29a}$$

For $\bar{\lambda}_z \geq D_3^*$ $$k_{zz}^* = C_{mz}\left[1 + D_1^*\left(D_3^* - D_2^*\right)n_z\right] \quad \text{Eq. 29b}$$

For $\bar{\lambda}_{z,csm} < D_{3,csm}^*$ $$k_{zz,csm}^* = C_{mz}\left[1 + D_{1,csm}^*\left(\bar{\lambda}_{z,csm} - D_{2,csm}^*\right)n_{z,csm}\right] \quad \text{Eq. 30a}$$

For $\bar{\lambda}_{z,csm} \geq D_{3,csm}^*$ $$k_{zz,csm}^* = C_{mz}\left[1 + D_{1,csm}^*\left(D_{3,csm}^* - D_{2,csm}^*\right)n_{z,csm}\right] \quad \text{Eq. 30b}$$

Following a similar procedure to that adopted for stocky cross-sections in Section 4.2, new D_i^* coefficients are proposed in this section to define the interaction factors for stainless steel beam-columns with slender cross-sections. While the modified $D_{i,csm}$ coefficients defined for stocky cross-sections compensated for the incorporation of strain hardening effects in the design resistances, the recalibrated D_i coefficients for slender cross-sections (D_i^* and $D_{i,csm}^*$) counteract the effect of local buckling in the calculation of the interaction factors k_{zz} and $k_{zz,csm}$ and lead to flexural buckling and bending moment interaction levels similar to those exhibited by equivalent fully effective cross-sections with no strain hardening. To achieve this, a new correction factor γ^*, given in Eq. 31, is defined for beam-columns with slender cross-section, which leads to the definition of the revised D_i^* and $D_{i,csm}^*$ coefficients given by Eq. 32 to Eq. 34. Note that in order to maintain consistency in the recalibrated $D_{i,csm}$ coefficients between stocky and slender sections, the definition of the γ and γ^* factors is different for the CSM approach. It is also important to highlight that the definition of the correction factor for slender cross-sections γ^* has an equivalent meaning regardless the adopted design approach (i.e. a cross-section effectiveness ratio), although the equations used in the calculation of these factors are different when the Eurocode 3 or CSM design approaches are adopted, using either the effective width equations [4] or the CSM base curve [30].

$$\gamma^* = \sqrt{A_{eff}/A} \quad \text{or} \quad \gamma^* = \sqrt{\sigma_{c,csm}/f_y} \qquad \text{Eq. 31}$$

$$D_1^* = \gamma^* D_1 \quad \text{or} \quad D_{1,csm}^* = \gamma^* D_1 \qquad \text{Eq. 32}$$

$$D_2^* = D_2/\gamma^* \quad \text{or} \quad D_{2,csm}^* = D_2/\gamma^* \qquad \text{Eq. 33}$$

$$D_3^* = D_3/\gamma^* \quad \text{or} \quad D_{3,csm}^* = D_3/\gamma^* \qquad \text{Eq. 34}$$

Assessment of the results corresponding to the interaction equation given in Eq. 21 and the new interaction factors defined in Eq. 29 and Eq. 30 is presented in Table 10, in which Design Approach C is based on the effective end-points calculated following the Effective Width Method [4] ($N_{b,eff,Rk}$ and $M_{c,eff,Rk}$) with the interaction factor defined in Eq. 29, while Design Approach D corresponds to the reduced CSM resistances ($N_{b,eff,csm,Rk}$ and $M_{c,eff,csm,Rk}$) [30] and the interaction factor in Eq. 30, as defined in Table 9. The results show that the improvement achieved in the prediction of the beam-column capacity for the recalibrated interaction factors k_{zz}^{*} and $k_{zz,csm}^{*}$ is limited, and similar for the Eurocode 3 and CSM design approaches, obtaining equivalent levels of accuracy for Design Approaches C and D. Similar observations can be made from Figures 9 to 11 for the different families of stainless steel. This can be explained by the considerable conservatism associated with the calculation of the end-points for members with slender cross-section, as shown by the interaction diagrams presented in Figure 12. These figures depict and compare the interaction curves corresponding to Design Approaches C and D with the experimental and numerical member capacity database in a normalized compression-bending interaction diagram. Note that although the specimens included in Figure 12 have different member slendernesses and levels of axial compression, and thus, different interaction diagrams apply, only the average interaction curves have been plotted for simplicity. The results in Figure 12 suggest that the flexural buckling and bending moment resistances acting as the end-points in these interaction diagrams should be revised in order to achieve more accurate beam-column ultimate load predictions, since the recalibration of new interaction factors is not sufficient to compensate for the underestimation of these end-points. This has been also highlighted in other studies into the resistance of stainless steel members with slender cross-sections [29,50,51].

6. RELIABILITY ANALYSIS

The reliability of the proposed CSM approach for the design of stainless steel SHS and RHS beam-columns is assessed in this section through statistical analyses. The reliability of the CSM design expressions in predicting the end points of the interaction curves has been demonstrated in previous studies [6,7,19,25-30], which have consistently shown that the CSM equations can be safely adopted with the γ_{M0} and γ_{M1} safety factors currently recommended in EN 1993-1-4 [4].

The statistical analyses for the different design approaches proposed in this paper for stainless steel members under combined loading have been carried out according to EN 1990, Annex D [52], although the method to calculate the mean value of the correlation factor b described in [53] has been adopted. The statistical parameters corresponding to the variation in geometrical properties for SHS and RHS specimens were taken from [54], while the variation in material properties for the different stainless steel families were extracted from [55]: yield overstrength ratios of 1.20, 1.15 and 1.10 for austenitic, ferritic and duplex families, respectively, with the corresponding coefficients of variation 0.059, 0.054 and 0.056. A summary of the most relevant statistical parameters for the different alternative design approaches considered in Sections 4 and 5 is presented in Table 11 and Table 12 for beam-columns with stocky and slender cross-sections, respectively. In these tables, n corresponds to the number of specimens, b is the mean value of the correction factor, V_δ is the coefficient of variation of the errors relative to the experimental results, V_r is the combined coefficient of variation and finally γ_{M1} is the calculated partial safety factor. Reliability analyses for the combined databases of members with both stocky and slender cross-sections are also reported in Table 13. According to the results reported in Table 11 to Table 13, the proposed CSM approaches for stainless steel beam-columns can be safely applied to members with both stocky and slender hollow sections, since the calculated γ_{M1} values lie below the partial safety factor γ_{M1} currently recommended in EN 1993-1-4 [4], equal to 1.10. It is worth noting that the γ_{M1} values reported in Table 13 for the CSM-based approaches when the full database is considered are slightly higher than the values calculated separately for stocky and slender cross-sections (see Table 11 and Table 12) because results are marginally more scattered, given the fact that greater improvements are obtained for members with stocky cross-sections when using CSM-based end-points than for members with slender cross-sections.

7. SUMMARY OF PROPOSALS

Based on the described analyses, the proposed CSM interaction factors $k_{zz,csm}$ for stainless steel SHS and RHS beam-columns with stocky and slender cross-sections (which correspond to Design Approaches 4 and D), to be used in conjunction with the interaction equation given in Eq. 21 are summarised as follows:

$$\text{For } \bar{\lambda}_{z,csm} < D_3/\gamma_{csm} \qquad k_{zz,csm} = C_{mz}\left[1 + \gamma_{csm} D_1\left(\bar{\lambda}_{z,csm} - D_2/\gamma_{csm}\right) n_{z,csm}\right] \qquad \text{Eq. 30a}$$

$$\text{For } \bar{\lambda}_{z,csm} \geq D_3/\gamma_{csm} \qquad k_{zz,csm} = C_{mz}\left[1 + \gamma_{csm} D_1 (D_3/\gamma_{csm} - D_2/\gamma_{csm}) n_{z,csm}\right] \qquad \text{Eq. 30b}$$

with

$$\gamma_{csm} = \begin{cases} \sqrt{f_y/\sigma_{c,csm}} & \text{for} \quad \bar{\lambda}_p \leq 0.68 \qquad \text{Eq. 25} \\ \sqrt{\sigma_{c,csm}/f_y} & \text{for} \quad \bar{\lambda}_p > 0.68 \qquad \text{Eq. 31} \end{cases}$$

And the proposed EN 1993-1-4 [4] interaction factors k_{zz} for stainless steel SHS and RHS beam-columns with slender cross-sections (corresponding to Design Approach C) are summarised as follows:

$$\text{For } \bar{\lambda}_z < D_3/\gamma_{EN} \qquad k_{zz} = C_{mz}\left[1 + \gamma_{EN} D_1\left(\bar{\lambda}_z - D_2/\gamma_{EN}\right) n_z\right] \qquad \text{Eq. 29a}$$

$$\text{For } \bar{\lambda}_z \geq D_3/\gamma_{EN} \qquad k_{zz} = C_{mz}[1 + \gamma_{EN} D_1 (D_3/\gamma_{EN} - D_2/\gamma_{EN}) n_z] \qquad \text{Eq. 29b}$$

with

$$\gamma_{EN} = \sqrt{A_{eff}/A} \qquad \text{Eq. 31}$$

and with the D_i coefficients given in Table 1.

8. WORKED EXAMPLE

This section provides a worked example illustrating the design of a stainless steel beam-column using the Continuous Strength Method. Design calculations are presented for a SHS 60×60×4 austenitic stainless steel member subjected to an eccentric compressive load, with a load eccentricity e_y of 18 mm. The ends of the beam-column are pinned about the z-z axis and fixed about the y-y axis. The geometric and material properties of one of the members simulated in the parametric study have been used and all factors of safety have been set to unity (i.e. characteristic resistances are considered), to allow a direct comparison with the FE result.

Geometric and material properties

$H = 60\ \mathrm{mm}$	$A = 827\ \mathrm{mm}^2$	$E = 200\ \mathrm{GPa}$
$B = 60\ \mathrm{mm}$	$I_z = 351780\ \mathrm{mm}^4$	$f_y = 499\ \mathrm{MPa}$
$t = 4\ \mathrm{mm}$	$W_{el,z} = 11726\ \mathrm{mm}^3$	$f_u = 728\ \mathrm{MPa}$
$R = 12\ \mathrm{mm}$	$W_{pl,z} = 16801\ \mathrm{mm}^3$	$\varepsilon_y = 499/200000 = 0.00250$
$L = 925\ \mathrm{mm}$	$e_y = 18\ \mathrm{mm}$	$\varepsilon_u = 1 - 499/728 = 0.315$
$\sigma_{cr,l,c} = 5014\ \mathrm{MPa}$	$\sigma_{cr,l,b} = 5565\ \mathrm{MPa}$	$N_{cr,z} = 811.6\ \mathrm{kN}$

Note that R is the external corner radius and $\sigma_{cr,l,c}$ and $\sigma_{cr,l,b}$ are the elastic local buckling stresses of the full cross-section in pure compression and pure bending, respectively, calculated using CUFSM [41]. The remaining parameters have been already defined in the previous sections of the paper.

Determine the CSM bending resistance $M_{c,csm,Rk}$

- Local cross-sectional slenderness in bending: $\bar{\lambda}_{p,b} = \sqrt{f_y/\sigma_{cr,l,b}} = \sqrt{499/5565} = 0.30$
- CSM base curve [6,13]: $\frac{\varepsilon_{csm}}{\varepsilon_y} = \frac{0.25}{\bar{\lambda}_{p,b}^{3.6}} = 19.1 > \min\left(15, \frac{0.1\varepsilon_u}{\varepsilon_y}\right) \therefore \frac{\varepsilon_{csm}}{\varepsilon_y} = 12.4$
- Strain hardening slope [6,13]: $E_{sh} = \frac{f_u - f_y}{0.16\varepsilon_u - \varepsilon_y} = 4780.8\ \mathrm{MPa}$
- CSM bending resistance: $M_{c,csm,Rk} = 9.96\ \mathrm{kNm}$ [prEN 1993-1-4 [13] predicted bending capacity is $M_{c,Rk} = 8.38\ \mathrm{kNm}$].

Determine the CSM compression resistance $N_{c,csm,Rk}$

- Local cross-sectional slenderness in compression: $\bar{\lambda}_{p,c} = \sqrt{f_y/\sigma_{cr,l,c}} = \sqrt{499/5014} = 0.315$
- CSM base curve [6,13]: $\frac{\varepsilon_{csm}}{\varepsilon_y} = \frac{0.25}{\bar{\lambda}_{p,c}^{3.6}} = 15.9 > \min\left(15, \frac{0.1\varepsilon_u}{\varepsilon_y}\right) \therefore \frac{\varepsilon_{csm}}{\varepsilon_y} = 12.4$
- CSM cross-section compression stress [6,13]: $\sigma_{c,csm} = f_y + E_{sh}\varepsilon_y\left(\frac{\varepsilon_{csm}}{\varepsilon_y} - 1\right) = 635.3\ \mathrm{MPa}$

- CSM cross-sectional compression resistance [6,13]: $N_{c,csm,Rk} = A\sigma_{c,csm} = 525.4$ kN

Determine the CSM flexural buckling resistance $N_{b,csm,Rk}$

- C_5 and C_6 coefficients: $C_6 = 1.2\left(f_u/f_y\right) = 1.75$ and $C_5 = 1 + 0.68C_6 = 2.19$
- CSM bow imperfection amplitude ratio: $e_{0,csm}/e_{0,el,EN} = C_5 - C_6\bar{\lambda}_{p,c} = 1.64$
- Equivalent CSM imperfection factor α_{csm}, using $\alpha_{EN} = 0.49$ for austenitic SHS members [13], $M_{el} = W_{el}f_y = 5.85$ kNm and $N_{pl} = Af_y = 412.7$ kN:

$$\alpha_{csm} = \alpha_{EN}\frac{e_{0,csm}}{e_{0,el,EN}}\sqrt{\frac{f_y}{\sigma_{c,csm}}\frac{N_{c,csm,Rk}M_{el}}{M_{c,csm,Rk}N_{pl}}} = 0.53$$

- CSM member slenderness: $\bar{\lambda}_{csm} = \sqrt{N_{c,csm,Rk}/N_{cr,z}} = \sqrt{525.4/811.6} = 0.80$
- Auxiliary factors ϕ_{csm} and χ_{csm}, using $\bar{\lambda}_0 = 0.3$ for austenitic SHS members [13]:

$$\phi_{csm} = 0.5\left[1 + \alpha_{csm}(\bar{\lambda}_{csm} - \bar{\lambda}_0) + \bar{\lambda}_{csm}^2\right] = 0.96$$

$$\chi_{csm} = \frac{1}{\phi_{csm} + \sqrt{\phi_{csm}^2 - \bar{\lambda}_{csm}^2}} = 0.68$$

- CSM flexural buckling resistance: $N_{b,csm,Rk} = \chi_{csm}N_{c,csm,Rk} = 355.5$ kN [prEN 1993-1-4 [13] predicted flexural buckling capacity is $N_{b,Rk} = 310.7$ kN].

Determine the ultimate CSM member capacity under combined load $N_{pred,csm}$

- CSM correction factor: since $\bar{\lambda}_{p,c} = 0.315 < 0.68$, $\gamma_{csm} = \sqrt{f_y/\sigma_{c,csm}} = 0.89$
- CSM beam-column check about the z-z axis:

$$\frac{N_{Ed}}{N_{b,csm,Rk}/\gamma_{M1}} + k_{zy,csm}\frac{M_{y,Ed} + \Delta M_{y,Ed}}{\chi_{LT}M_{y,csm,Rk}/\gamma_{M1}} + k_{zz,csm}\frac{M_{z,Ed} + \Delta M_{z,Ed}}{M_{z,csm,Rk}/\gamma_{M1}} \leq 1.0$$

with $k_{zz,csm} = C_{mz}\left[1 + \gamma_{csm}D_1\left(\bar{\lambda}_{z,csm} - D_2/\gamma_{csm}\right)n_{z,csm}\right]$

In this example $M_{y,Ed} = 0$, $M_{z,Ed} = N_{Ed}e_y$, $\Delta M_{z,Ed} = 0$, $C_{mz} = 1.0$ for uniform bending, $n_{csm} = N_{Ed}/N_{b,csm,Rk}$ and $\gamma_{M1} = 1.0$. Recall that γ_{M1} is equal to 1.10 for the design of stainless steel members, but is taken as 1.0 in this example to allow a direct comparison with the FE result.

- Setting $N_{Ed} = N_{pred,csm}$ and $M_{z,Ed} = N_{pred,csm} e_y$, the maximum compressive load that the member can attain can be determined by equating the above interaction expression to unity, hence:

$$\frac{N_{pred,csm}}{N_{b,csm,Rk}} + \left[1 + \gamma_{csm} D_1 \left(\bar{\lambda}_{csm} - D_2/\gamma_{csm}\right) \frac{N_{pred,csm}}{N_{b,csm,Rk}}\right] \frac{N_{pred,csm} e_y}{M_{z,csm,Rk}} = 1.0$$

$$\frac{N_{pred,csm}}{355.5} + \left[1 + 0.89 \cdot 2(0.80 - 0.3/0.89) \frac{N_{pred,csm}}{355.5}\right] \frac{N_{pred,csm} 0.018}{9.96} = 1.0$$

Then $N_{pred,csm} = 185.3$ kN [FE beam-column capacity is $N_{u,FE} = 211.2$ kN and the prEN 1993-1-4 [13] predicted beam-column capacity using Design Approach 1 is $N_{pred,EN} = 159.4$ kN].

9. CONCLUSIONS

Extension of the Continuous Strength Method (CSM) to the design of stainless steel SHS and RHS members subjected to combined compression and bending moment, utilising the formulation proposed in [19], is proposed herein. The method incorporates the effect of strain hardening in the prediction of the capacity of beam-columns with stocky cross-sections while otherwise maintaining the traditional design framework, and provides a simpler and more direct design approach for beam-columns with slender cross-sections. The accuracy of the proposed design approach has been assessed through comparison of the predicted resistances with experimental and numerical beam-column capacities for members with both stocky and slender cross-sections.

The comparisons show that the adoption of accurate CSM compression and bending end-points, in conjunction with existing interaction equations from the literature [11,22], which will be included in the upcoming version of the European design Standard for stainless steel structures prEN 1993-1-4 [13], provides more accurate beam-column strength predictions than existing provisions for members with stocky cross-sections, especially for combined loading conditions dominated by compression. The paper also presents a recalibration of the coefficients defining the current interaction equation to adapt it to the modified member slenderness and flexural buckling resistance calculations based on the CSM approach, which leads to yet more accurate predictions and provides a consistent level of accuracy across all three families of stainless steel. The equivalent analysis for beam-columns with slender cross-sections shows that similar resistance predictions are obtained for the EN 1993-1-4 [4] and the CSM design approaches, although the need for more accurate resistance functions to predict the end-points for such members is also highlighted. A reliability analysis, carried out according to EN 1990, Annex D [52], indicates that the proposed design approaches can be safely applied with the currently recommended partial safety factor $\gamma_{M1} = 1.10$ for the design of stainless steel SHS and RHS beam-columns with stocky and slender cross-sections.

ACKNOWLEDGEMENTS

Funding for this investigation was received from the Spanish Ministerio de Educación, Cultura y Deporte through the José Castillejo-2018 scholarship.

REFERENCES

[1] Baddoo, N.R. (2008) Stainless steel in construction: A review of research, applications, challenges and opportunities. *Journal of Constructional Steel Research* 64(11), 1199–1206.

[2] Cashell, K.A. and Baddoo, N.R. (2014) Ferritic stainless steels in structural applications. *Thin-Walled Structures* 83, 169–181.

[3] Gardner, L. (2019) Stability and design of stainless steel structures – Review and outlook. *Thin-Walled Structures* 141, 208–216.

[4] European Committee for Standardization (CEN) (2015) EN 1993-1-4:2006+A1:2015. Eurocode 3: Design of Steel Structures – Part 1-4: General Rules. Supplementary Rules for Stainless Steels, including amendment A1. Brussels, Belgium.

[5] European Committee for Standardization (CEN) (2005) EN 1993-1-1. Eurocode 3: Design of Steel Structures – Part 1-1: General rules and rules for buildings. Brussels, Belgium.

[6] Afshan, S. and Gardner, L. (2013) The continuous strength method for structural stainless steel design. *Thin-Walled Structures* 68, 42–49.

[7] Bock, M., Gardner, L. and Real, E. (2015) Material and local buckling response of cold-formed ferritic stainless steel sections. *Thin-Walled Structures* 89, 131–141.

[8] Yun, X. and Gardner, L. (2018) The continuous strength method for the design of cold-formed steel non-slender tubular cross-sections. *Engineering Structures* 175, 549–564.

[9] Gardner, L., Wang, F. and Liew, A. (2011) Influence of strain hardening on the behavior and design of steel structures. *International Journal of Structural Stability and Dynamics* 11(5), 855–875.

[10] Su, M., Young, B. and Gardner, L. (2016) The continuous strength method for the design of aluminium alloy structural elements. *Engineering Structures* 122, 338–348.

[11] Steel Construction Institute (SCI) (2017) Design Manual for Structural Stainless Steel. 4th Edition.

[12] American Institute of Steel Construction (AISC). (2013) Design Guide 27: Structural Stainless Steel. Illinois, USA.

[13] prEN 1993-1-4 (2020) Eurocode 3: Design of Steel Structures – Part 1-4: General Rules. Supplementary rules for stainless steels. Second draft.

[14] American Society of Civil Engineers (ASCE). (2021) Specification for the Design of Cold-Formed Stainless Steel Structural Members. SEI/ASCE 8-21. Virginia, USA.

[15] American Institute of Steel Construction (ANSI/AISC). (2021). Specification for Structural Steel Buildings. AISC 370-21. Illinois, USA.

[16] Fieber, A., Gardner, L. and Macorini, L. (2019). Design of structural steel members by advanced inelastic analysis with strain limits. *Engineering Structures* 199, 109624.

[17] Fieber, A., Gardner, L. and Macorini, L. (2020) Structural steel design using second-order inelastic analysis with strain limits. *Journal of Constructional Steel Research* 168, 105980.

[18] Walport, F., Gardner, L. and Nethercot, D.A. (2020) Equivalent bow imperfections for use in design by second order inelastic analysis. *Structures* 26, 670–685.

[19] Arrayago, I., Real, E. and Mirambell, E; Gardner, L. (2020) The Continuous Strength Method for the design of stainless steel hollow section columns. *Thin-Walled Structures* 154, 106825.

[20] Arrayago, I. and Real, E. (2015) Experimental study on ferritic stainless steel RHS and SHS cross-sectional resistance under combined loading. *Structures* 4, 69–79.

[21] Zhao, O., Rossi, B., Gardner, L. and Young, B. (2015) Behaviour of structural stainless steel cross-sections under combined loading – Part II: Numerical modelling and design approach. *Engineering Structures* 89, 247–259.

[22] Zhao, O., Gardner, L. and Young, B. (2016) Behaviour and design of stainless steel SHS and RHS beam-columns. *Journal of Constructional Steel Research* 106, 330–345.

[23] Arrayago, I., Rasmussen, K.J.R. and Real, E. (2017) Full slenderness range DSM approach for stainless steel hollow cross-section columns and beam-columns. *Journal of Constructional Steel Research* 138, 246–263.

[24] Afshan, S., Zhao, O. and Gardner L. (2019) Standardised material properties for numerical parametric studies of stainless steel structures and buckling curves for tubular columns. *Journal of Constructional Steel Research* 152, 2–11.

[25] Zhao, O., Rossi, B., Gardner, L. and Young, B. (2015) Behaviour of structural stainless steel cross-sections under combined loading – Part I: Experimental study, *Engineering Structures* 89, 236–246.

[26] Zhao, O., Rossi, B., Gardner, L. and Young, B. (2015) Experimental and Numerical Studies of Ferritic Stainless Steel Tubular Cross Sections under Combined Compression and Bending. *Journal of Structural Engineering (ASCE)*, 04015110-2.

[27] Arrayago, I. and Real, E. (2016) Experimental study on ferritic stainless steel simply supported and continuous beams. Journal of Constructional Steel Research 119, 50–62.

[28] Arrayago, I., Real, E. and Mirambell, E. (2017) Design of stainless steel continuous beams with tubular cross-sections. *Engineering Structures* 151, 422–431.

[29] Arrayago, I., Rasmussen, K.J.R. and Real, E. (2017) Full slenderness range DSM approach for stainless steel hollow cross-sections. *Journal of Constructional Steel Research* 133, 156–166.

[30] Zhao, O., Afshan, S. and Gardner, L. (2017) Structural response and continuous strength method design of slender stainless steel cross-sections. *Engineering Structures* 140, 14–25.

[31] Steel Construction Institute (SCI) (2017) Design Manual for Structural Stainless Steel - Commentary. 4th Edition.

[32] prEN 1993-1-1 (2019) Eurocode 3: Design of Steel Structures – Part 1-1: General rules and rules for buildings. Final Document.

[33] Kucukler, M., Gardner, L. and Bu, Y. (2020) Flexural-torsional buckling of stainless steel I-section beam-columns: Testing, numerical modelling and design, *Thin-Walled Structures* 152, 106572.

[34] Talja, A. and Salmi, P. (1995) Design of stainless steel RHS beams, columns and beam columns. Research Note 1619, VTT-Building Technology. Finland.

[35] Hyttinen, V. (1994) Design of cold-formed stainless steel SHS beam-columns. Research report 41, University of Oulu. Finland.

[36] Zheng, B., Hua, X. and Shu, G. (2015) Tests of cold-formed and welded stainless steel beam-columns. *Journal of Constructional Steel Research* 111, 1–10.

[37] Zhao, O., Gardner, L. and Young, B. (2016) Buckling of ferritic stainless steel members under combined axial compression and bending. *Journal of Constructional Steel Research* 117, 35–48.

[38] Arrayago, I., Real, E. and Mirambell, E. (2016) Experimental study on ferritic stainless steel RHS and SHS beam-columns. *Thin-Walled Structures* 100, 93–104.

[39] Lui, W.M., Ashraf, M. and Young, B. (2014) Tests of cold-formed duplex stainless steel SHS beam-columns. *Engineering Structures* 74, 111–121.

[40] Huang, Y. and Young, B. (2014) Experimental investigation of cold-formed lean duplex stainless steel beam-columns. *Thin-Walled Structures* 76, 105–117.

[41] Li, Z. and Schafer, B.W. (2010) Buckling analysis of cold-formed steel members with general boundary conditions using CUFSM: conventional and constrained finite strip methods. *Twentieth International Speciality Conference on Cold-Formed Steel Structures*. Saint Louis, USA.

[42] Gardner, L., Fieber, A. and Macorini, L. (2019) Formulae for calculating elastic local buckling stresses of full structural cross-sections. *Structures* 17, 2–20.

[43] ABAQUS (2014) ABAQUS/Standard user's manual volumes I-III and ABAQUS CAE manual. Dassault Systemes Simulia Corporation.

[44] Becque, J. (2008) The interaction of local and overall buckling of cold-formed stainless steel columns. PhD. Thesis. School of Civil Engineering, The University of Sydney, Australia.

[45] Gardner, L. and Cruise, R.B. (2009) Modeling of residual stresses in structural stainless steel sections. *Journal of Structural Engineering (ASCE)* 135(1), 42–53.

[46] Jandera, M., Gardner, L. and Machacek, J. (2008) Residual stresses in cold-rolled stainless steel hollow sections. *Journal of Constructional Steel Research* 64 (11), 1255–1263.

[47] Rasmussen, K.J.R. and Hancock, G.J. (1993) Design of cold-formed stainless steel tubular members. I: Columns. *Journal of Structural Engineering (ASCE)* 119(8), 2349–2367.

[48] Arrayago, I., Real, E. and Gardner, L. (2015) Description of stress-strain curves for stainless steel alloys. *Materials & Design* 87, 540–552.

[49] Gardner L. and Nethercot D.A. (2004) Numerical modeling of stainless steel structural components – A consistent approach. *Journal of Structural Engineering (ASCE)*, 130(10), 1586–1601.

[50] Becque, J. and Rasmussen, K.J.R. (2009) Numerical investigation of the interaction of local and overall buckling of stainless steel I-columns. *Journal of Structural Engineering (ASCE)* 135(11), 1349–1356.

[51] Huang, Y. and Young, B. (2012) Material properties of cold-formed lean duplex stainless steel sections. *Thin-Walled Structures* 54, 72–81.

[52] European Committee for Standardization (CEN) (2005) EN 1990:2005. Eurocode 0. Basis of structural design. Brussels, Belgium.

[53] Bu, Y. and Gardner, L. (2019) Laser-welded stainless steel I-section beam-columns: Testing, simulation and design. *Engineering Structures* 179, 23–36.

[54] Afshan, S., Francis, P., Baddoo, N.R. and Gardner, L. (2015) Reliability analysis of structural stainless steel design provisions. *Journal of Constructional Steel Research* 114, 293–304.

[55] Steel Construction Institute (SCI) (2020) Proposed material factors for EN 1993-1-4. Technical Report. UK.

FIGURES

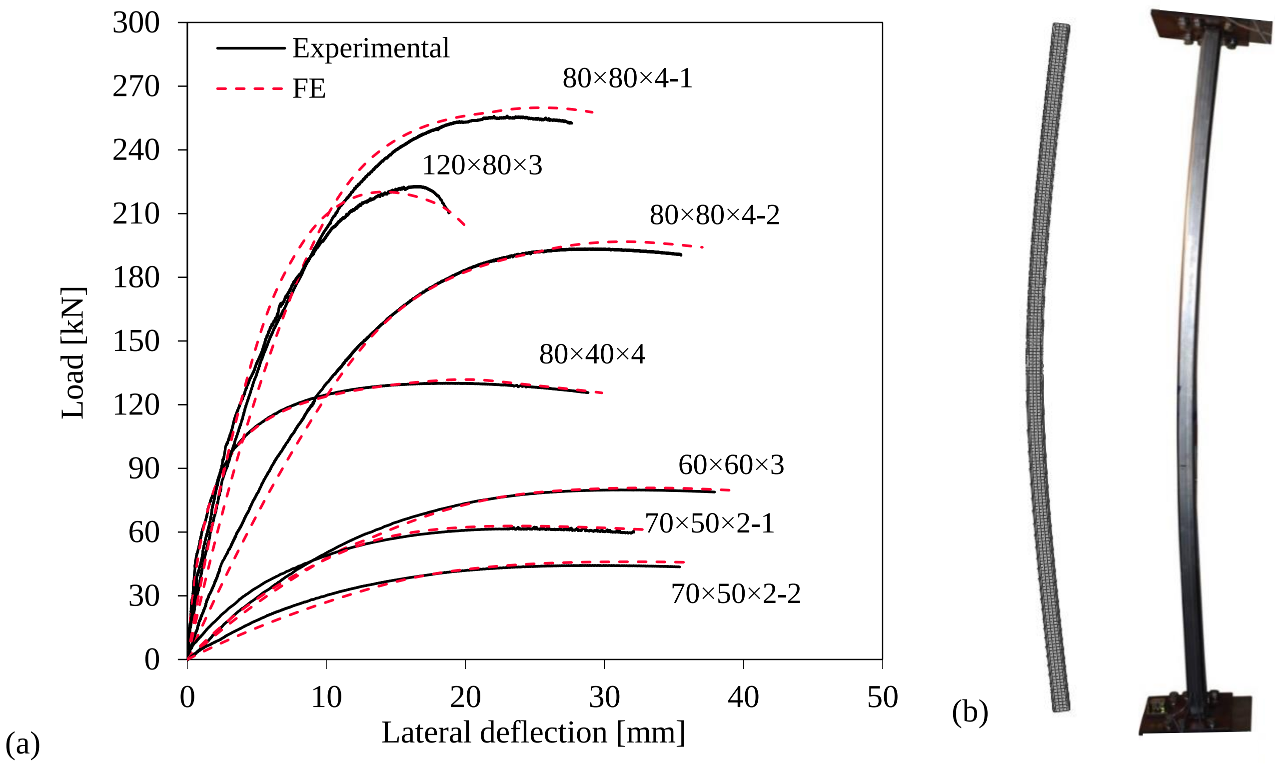

Figure 1. Comparison of experimental and numerical a) load–mid-height lateral deflection curves, and b) failure modes for typical beam-column specimens [38].

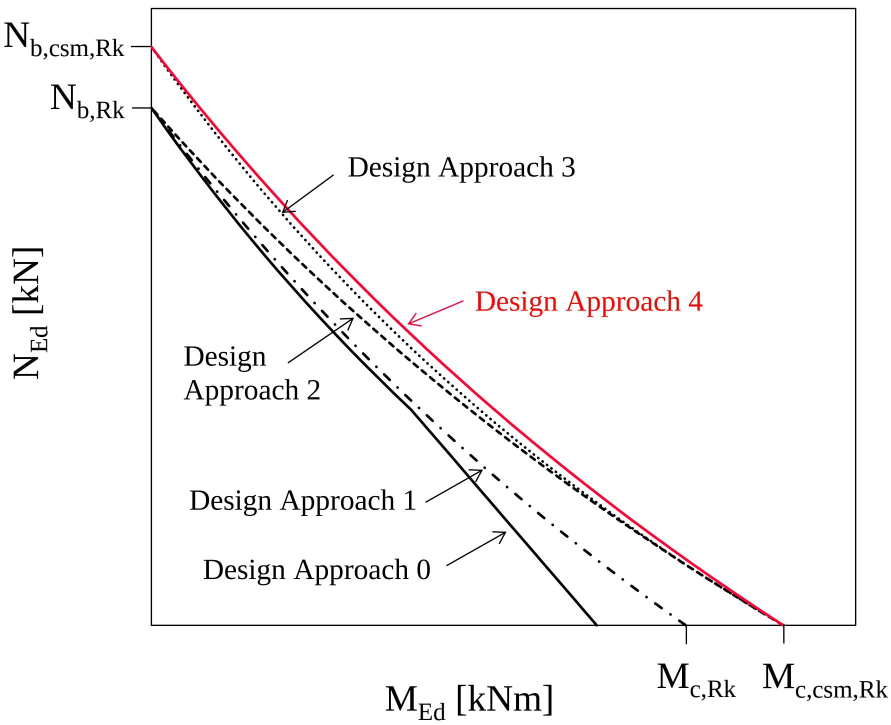

Figure 2. Graphical illustration of the different approaches considered for the design of stainless steel beam-columns with stocky cross-sections using different end-points.

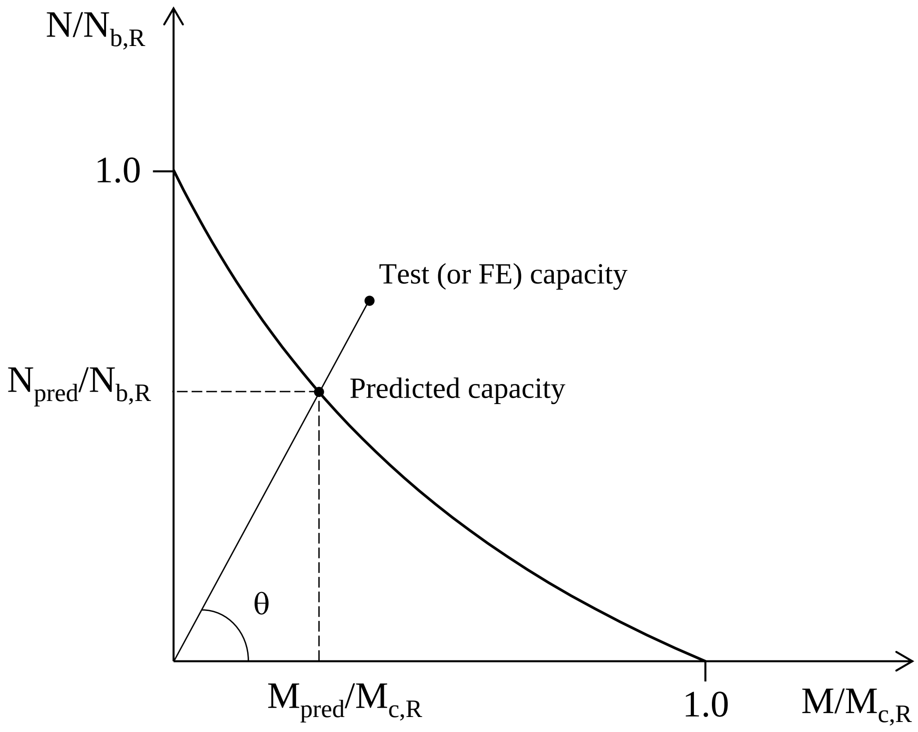

Figure 3. Definition of θ on axial load-moment interaction curve.

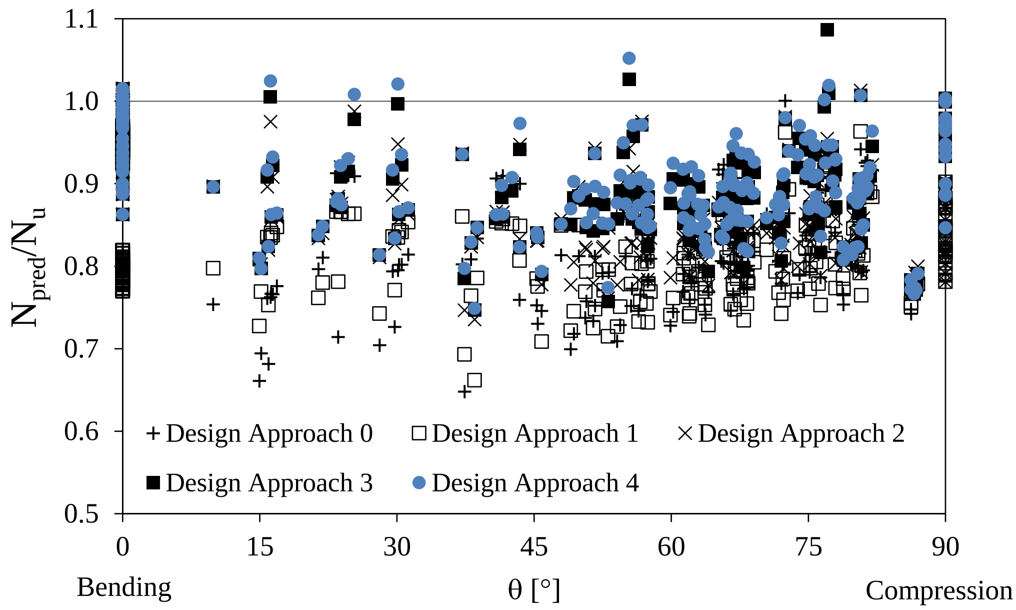

Figure 4. Predicted-to-ultimate resistance ratios obtained using the different design approaches for austenitic stainless steel members with stocky cross-sections under combined loading.

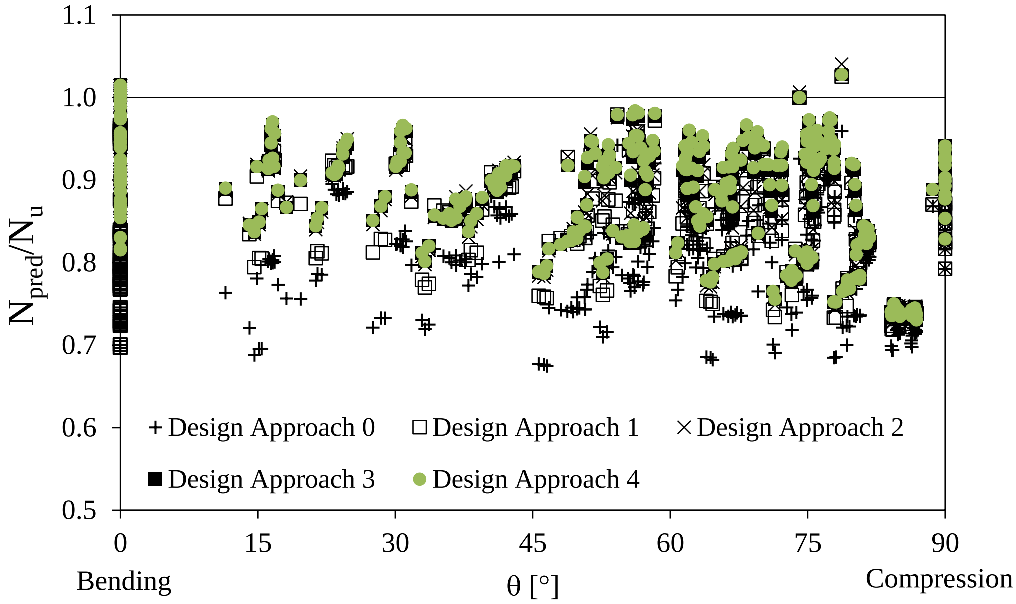

Figure 5. Predicted-to-ultimate resistance ratios obtained using the different design approaches for ferritic stainless steel members with stocky cross-sections under combined loading.

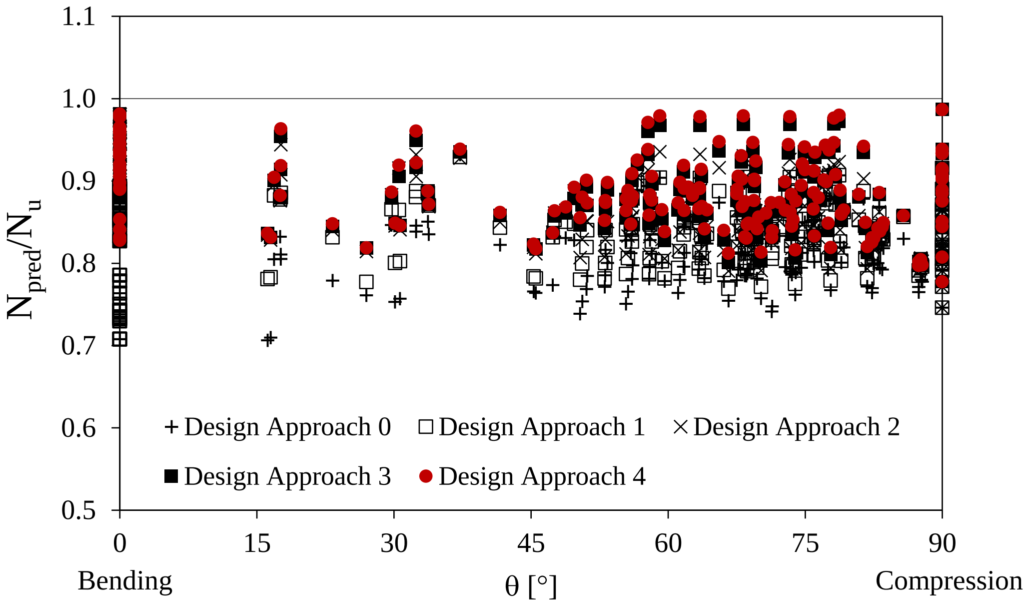

Figure 6. Predicted-to-ultimate resistance ratios obtained using the different design approaches for duplex stainless steel members with stocky cross-sections under combined loading.

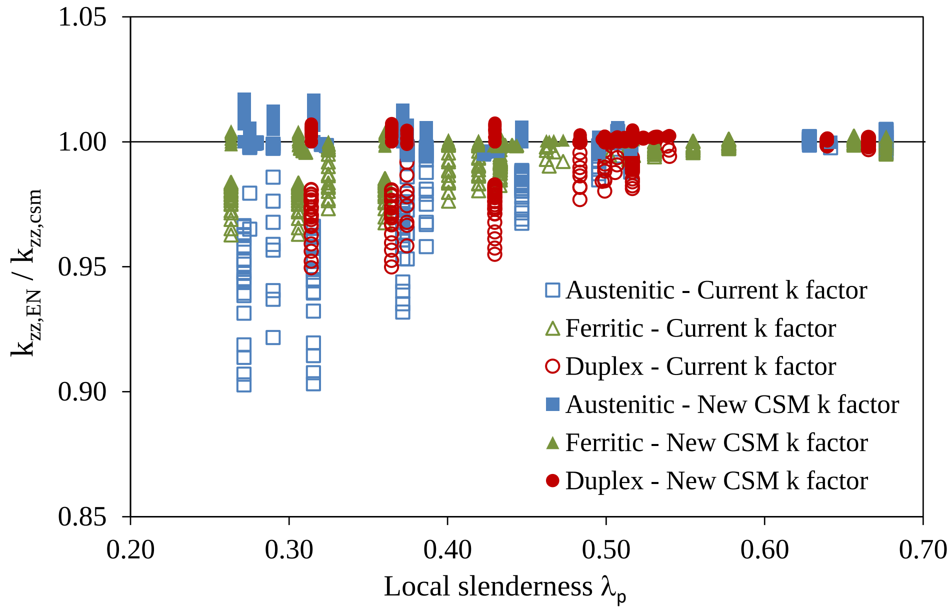

Figure 7. Comparison between the interaction factors obtained using the original D_i values and the new $D_{i,csm}$ values.

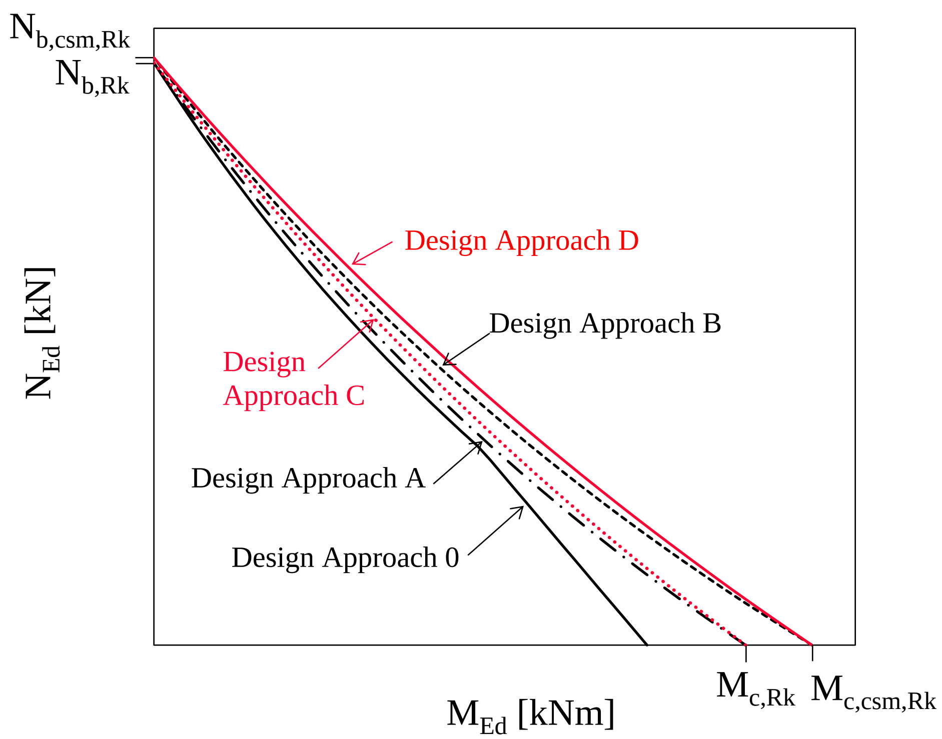

Figure 8. Graphical illustration of the different design approaches considered for the design of stainless steel beam-columns with slender cross-sections using different end-points.

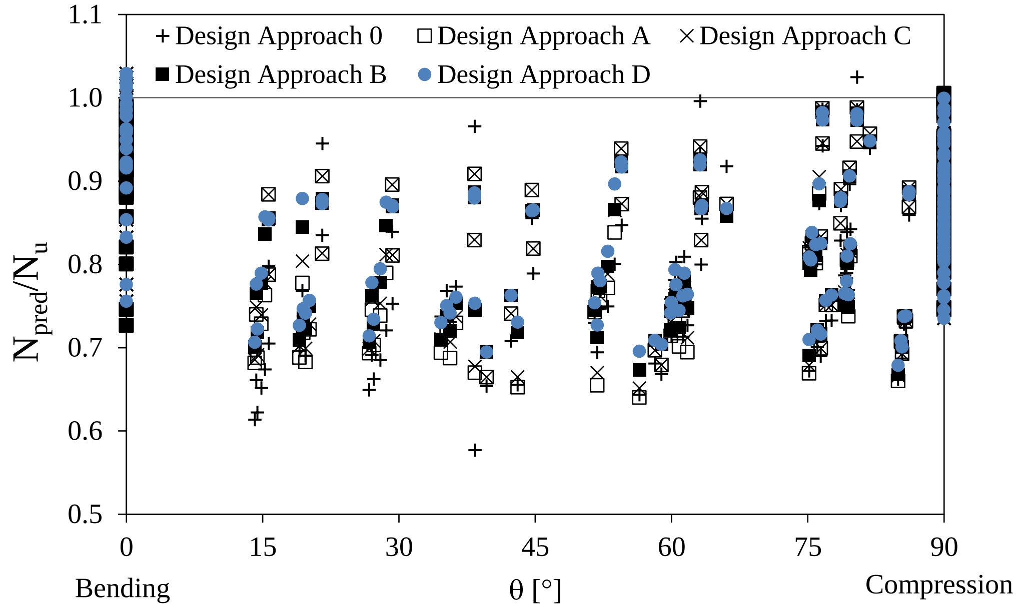

Figure 9. Predicted-to-ultimate resistance ratios obtained using the different design approaches for austenitic stainless steel members with slender cross-sections under combined loading.

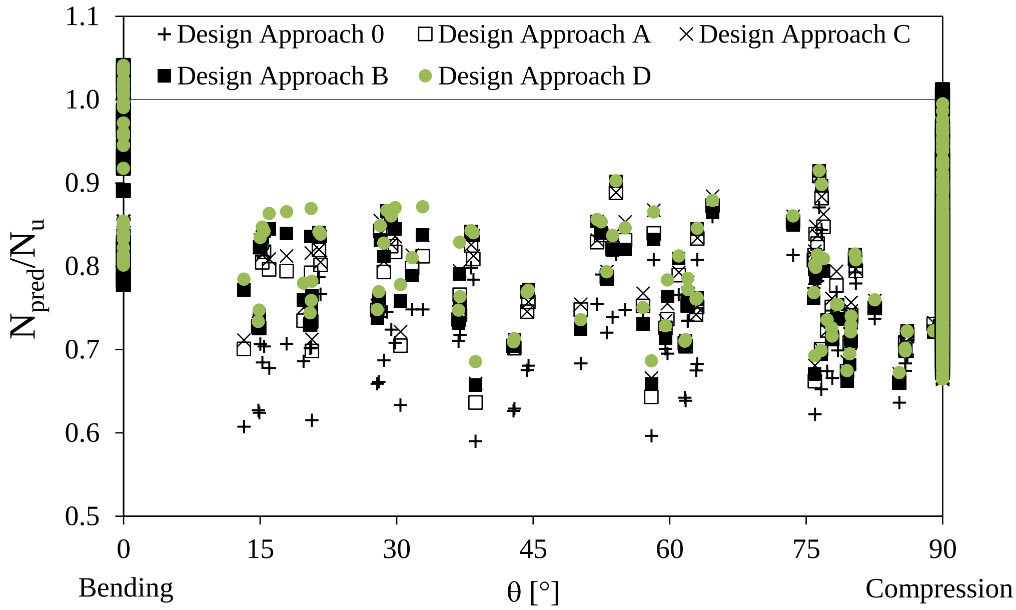

Figure 10. Predicted-to-ultimate resistance ratios obtained using the different design approaches for ferritic stainless steel members with slender cross-sections under combined loading.

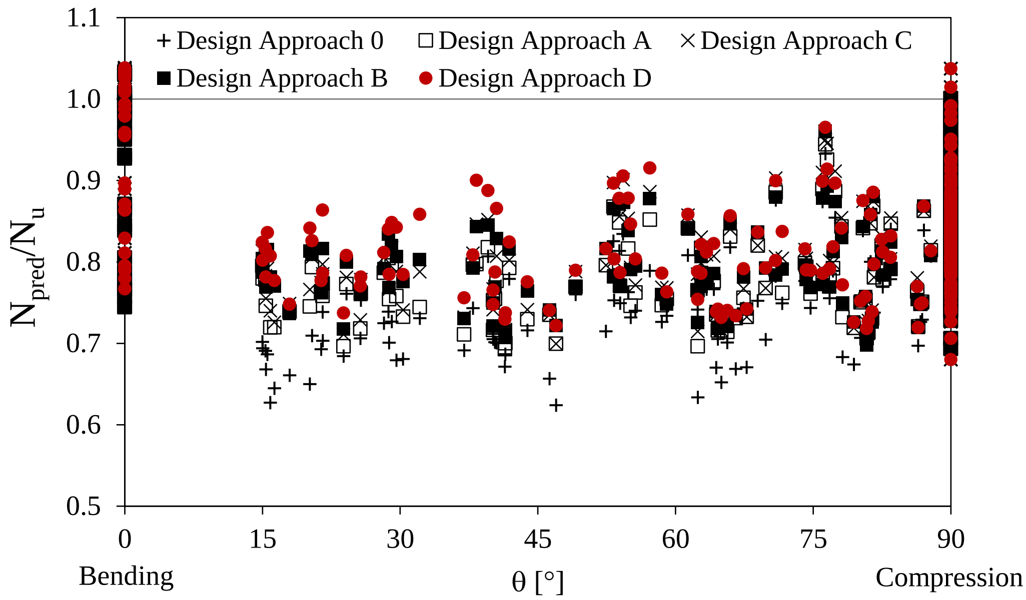

Figure 11. Predicted-to-ultimate resistance ratios obtained using the different design approaches for duplex stainless steel members with slender cross-sections under combined loading.

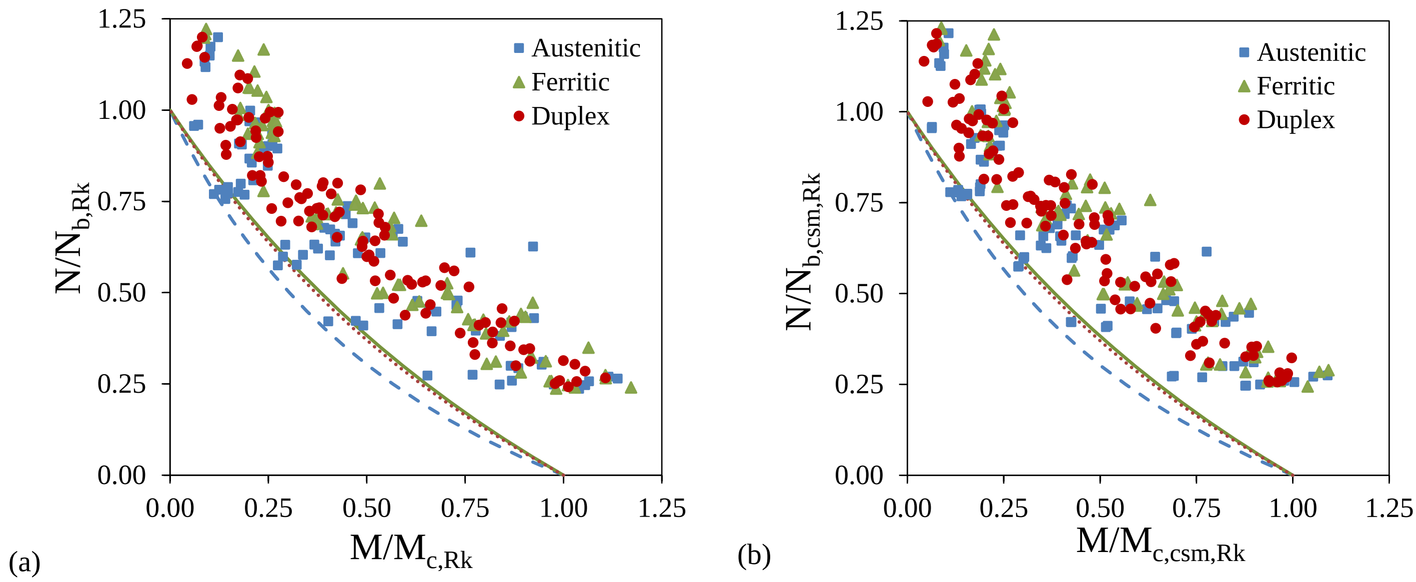

Figure 12. Comparison of interaction curves with the revised interaction factors against experimental and FE resistances of beam-columns with slender cross-sections for (a) Design Approach C and (b) Design Approach D.

TABLES

Table 1. D_1, D_2 and D_3 coefficients for stainless steel SHS and RHS beam-columns.

Stainless steel family	$\mathbf{D_1}$	$\mathbf{D_2}$	$\mathbf{D_3}$
Austenitic	2.00	0.30	1.3
Ferritic	1.30	0.45	1.6
Duplex	1.50	0.40	1.4

Table 2. Interaction factors k_{yy} and k_{yz} for instability governed by buckling about the y-y axis for rectangular hollow sections [13].

Austenitic	Duplex	Ferritic
For $\bar{\lambda}_y < 1.3$: $k_{yy} = C_{my}\left[1 + 2.00\left(\bar{\lambda}_y - 0.30\right)n_y\right]$	For $\bar{\lambda}_y < 1.4$: $k_{yy} = C_{my}\left[1 + 1.50\left(\bar{\lambda}_y - 0.40\right)n_y\right]$	For $\bar{\lambda}_y < 1.6$: $k_{yy} = C_{my}\left[1 + 1.30\left(\bar{\lambda}_y - 0.45\right)n_y\right]$
For $\bar{\lambda}_y \geq 1.3$: $k_{yy} = C_{my}\left(1 + 2.00n_y\right)$	For $\bar{\lambda}_y \geq 1.4$: $k_{yy} = C_{my}\left(1 + 1.5n_y\right)$	For $\bar{\lambda}_y \geq 1.6$: $k_{yy} = C_{my}\left(1 + 1.495n_y\right)$
$k_{yz} = k_{zz}$ (for k_{zz} see Table 3)		

Table 3. Interaction factors k_{zy} and k_{zz} for instability governed by buckling about the z-z axis for rectangular hollow sections [13].

Austenitic	Duplex	Ferritic
$k_{zy} = k_{yy}$ (for k_{yy} see Table 2)		
For $\bar{\lambda}_z < 1.3$: $k_{zz} = C_{mz}\left[1 + 2.00\left(\bar{\lambda}_z - 0.30\right)n_z\right]$	For $\bar{\lambda}_z < 1.4$: $k_{zz} = C_{mz}\left[1 + 1.50\left(\bar{\lambda}_z - 0.40\right)n_z\right]$	For $\bar{\lambda}_z < 1.6$: $k_{zz} = C_{mz}\left[1 + 1.30\left(\bar{\lambda}_z - 0.45\right)n_z\right]$
For $\bar{\lambda}_z \geq 1.3$: $k_{zz} = C_{mz}(1 + 2.00n_z)$	For $\bar{\lambda}_z \geq 1.4$: $k_{zz} = C_{mz}(1 + 1.5n_z)$	For $\bar{\lambda}_z \geq 1.6$: $k_{zz} = C_{mz}(1 + 1.495n_z)$

Table 4. Assembled experimental results on stainless steel hollow section beam-columns.

Stainless steel family	Cross-section type	No. of tests	Range of cross-section slenderness	Range of member slenderness	Reference
Austenitic	Stocky sections	8	0.28-0.51	0.68-1.50	[34]
		9	0.28-0.43	1.94-3.23	[35]
		1	0.64	1.28	[36]
	Slender sections	4	0.90	0.56-1.23	[34]
		4	0.80	0.99-2.13	[35]
Ferritic	Stocky sections	6	0.46-0.47	0.53	[37]
		4	0.47-0.52	0.93-1.75	[38]
		11	0.31-0.44	2.19-3.09	[35]
	Slender sections	6	1.17	0.51	[37]
		3	0.86-0.95	0.71-1.21	[38]
Duplex	Stocky sections	7	0.52-0.54	0.76-1.43	[39]
		9	0.50-0.51	0.62-1.58	[40]
	Slender sections	8	1.00	0.51-0.96	[39]
		28	1.00-1.60	0.43-1.36	[40]

Table 5. Comparison between experimental and FE results for stainless steel beam-columns [38].

Section	$N_{u,FE}/N_{u,exp}$	$\delta_{u,FE}/\delta_{u,exp}$
80×80×4-1	1.02	1.08
80×80×4-2	1.02	1.04
60×60×3	1.01	1.02
80×40×4	1.03	1.03
120×80×3	0.99	0.87
70×50×2-1	1.01	0.96
70×50×2-2	1.04	1.03
Mean	1.02	1.00
COV	0.017	0.070

Table 6. Basic material parameters adopted in the parametric study for different stainless steel families.

Stainless steel family	Section region	$\boldsymbol{E}$ [GPa]	$\boldsymbol{f_y}$ [MPa]	$\boldsymbol{f_u}$ [MPa]	$\boldsymbol{\varepsilon_u}$ [mm/mm]	$\boldsymbol{n}$ [-]	$\boldsymbol{m}$ [-]
Austenitic	Flat	200	460	700	0.20	7.1	2.9
	Corner	200	640	830	0.20	6.4	7.1
Ferritic	Flat	200	430	490	0.06	11.5	4.6
	Corner	200	560	610	0.01	5.7	6.8
Duplex	Flat	200	630	780	0.13	7.5	4.8
	Corner	200	800	980	0.03	6.1	6.7

Table 7. Summary of different approaches considered for the design of stainless steel beam-columns with stocky cross-sections.

Design approach	Flexural buckling resistance	Bending moment resistance	Interaction equation	Interaction factor
Design Approach 0	$N_{b,Rk}$	$M_{c,Rk}$	Eq. 14	Eq. 15
Design Approach 1	$N_{b,Rk}$	$M_{c,Rk}$	Eq. 21	Eq. 22
Design Approach 2	$N_{b,Rk}$	$M_{c,csm,Rk}$	Eq. 21	Eq. 22
Design Approach 3	$N_{b,csm,Rk}$	$M_{c,csm,Rk}$	Eq. 21	Eq. 22
Design Approach 4	$N_{b,csm,Rk}$	$M_{c,csm,Rk}$	Eq. 21	Eq. 24

Table 8. Assessment of the influence of different end-points in the prediction of the resistance of stainless steel members with stocky cross-sections under combined loading.

Design approach	Stainless steel family	Loading type $0^o \leq \theta < 45^o$		Loading type $45^o \leq \theta \leq 90^o$		Loading type $0^o \leq \theta \leq 90^o$	
		N_{pred}/N_u Mean	N_{pred}/N_u COV	N_{pred}/N_u Mean	N_{pred}/N_u COV	N_{pred}/N_u Mean	N_{pred}/N_u COV
Design Approach 0 (Interaction factor: Eq. 15 End-points: $N_{b,Rk}$, $M_{c,Rk}$)	Austenitic	0.797	0.109	0.821	0.069	0.817	0.078
	Ferritic	0.808	0.065	0.802	0.081	0.803	0.077
	Duplex	0.808	0.067	0.818	0.052	0.817	0.054
Design Approach 1 (Interaction factor: Eq. 22 End-points: $N_{b,Rk}$, $M_{c,Rk}$)	Austenitic	0.813	0.065	0.811	0.064	0.812	0.064
	Ferritic	0.879	0.053	0.841	0.074	0.850	0.072
	Duplex	0.852	0.051	0.833	0.044	0.835	0.045
Design Approach 2 (Interaction factor: Eq. 22 End-points: $N_{b,Rk}$, $M_{c,csm,Rk}$)	Austenitic	0.870	0.064	0.842	0.056	0.847	0.059
	Ferritic	0.892	0.043	0.850	0.074	0.860	0.071
	Duplex	0.877	0.044	0.848	0.043	0.851	0.044
Design Approach 3 (Interaction factor: Eq. 22 End-points: $N_{b,csm,Rk}$, $M_{c,csm,Rk}$)	Austenitic	0.874	0.065	0.881	0.063	0.880	0.064
	Ferritic	0.893	0.043	0.866	0.084	0.872	0.077
	Duplex	0.882	0.046	0.875	0.049	0.875	0.049
Design Approach 4 (Interaction factor: Eq. 24 End-points: $N_{b,csm,Rk}$, $M_{c,csm,Rk}$)	Austenitic	0.881	0.072	0.890	0.063	0.889	0.065
	Ferritic	0.898	0.043	0.868	0.085	0.874	0.078
	Duplex	0.886	0.049	0.880	0.050	0.880	0.050

Table 9. Summary of design approaches considered for the design of stainless steel beam-columns with slender cross-sections.

Design approach	Flexural buckling resistance	Bending moment resistance	Interaction equation	Interaction factors
Design Approach 0	$N_{b,eff,Rk}$	$M_{c,eff,Rk}$	Eq. 14	Eq. 15
Design Approach A	$N_{b,eff,Rk}$	$M_{c,eff,Rk}$	Eq. 21	Eq. 22
Design Approach B	$N_{b,eff,csm,Rk}$	$M_{c,eff,csm,Rk}$	Eq. 21	Eq. 22
Design Approach C	$N_{b,eff,Rk}$	$M_{c,eff,Rk}$	Eq. 21	Eq. 29
Design Approach D	$N_{b,eff,csm,Rk}$	$M_{c,eff,csm,Rk}$	Eq. 21	Eq. 30

Table 10. Assessment of the influence of different end-points in the prediction of the resistance of stainless steel members with slender cross-sections under combined loading.

Design approach	Stainless steel family	Loading type $0^o \leq \theta < 45^o$		Loading type $45^o \leq \theta \leq 90^o$		Loading type $0^o \leq \theta \leq 90^o$	
		N_{pred}/N_u Mean	N_{pred}/N_u COV	N_{pred}/N_u Mean	N_{pred}/N_u COV	N_{pred}/N_u Mean	N_{pred}/N_u COV
Design Approach 0	Austenitic	0.735	0.090	0.800	0.095	0.776	0.098
(Interaction factor: Eq. 15	Ferritic	0.696	0.053	0.731	0.063	0.717	0.062
End-points: $N_{b,eff,Rk}$, $M_{c,eff,Rk}$)	Duplex	0.707	0.039	0.760	0.065	0.741	0.062
Design Approach A	Austenitic	0.757	0.075	0.796	0.092	0.782	0.088
(Interaction factor: Eq. 22	Ferritic	0.767	0.050	0.768	0.064	0.768	0.058
End-points: $N_{b,eff,Rk}$, $M_{c,eff,Rk}$)	Duplex	0.757	0.033	0.788	0.057	0.777	0.052
Design Approach B	Austenitic	0.786	0.066	0.806	0.087	0.799	0.080
(Interaction factor: Eq. 22	Ferritic	0.789	0.052	0.763	0.065	0.773	0.061
End-points: $N_{b,eff,csm,Rk}$, $M_{c,eff,csm,Rk}$)	Duplex	0.783	0.037	0.792	0.055	0.789	0.049
Design Approach C	Austenitic	0.764	0.072	0.802	0.090	0.788	0.086
(Interaction factor: Eq. 29	Ferritic	0.777	0.050	0.775	0.064	0.771	0.064
End-points: $N_{b,eff,Rk}$, $M_{c,eff,Rk}$)	Duplex	0.775	0.036	0.801	0.060	0.792	0.054
Design Approach D	Austenitic	0.794	0.064	0.814	0.084	0.806	0.078
(Interaction factor: Eq. 30	Ferritic	0.801	0.053	0.772	0.064	0.784	0.062
End-points: $N_{b,eff,csm,Rk}$, $M_{c,eff,csm,Rk}$)	Duplex	0.804	0.043	0.807	0.058	0.806	0.053

Table 11. Summary of the reliability analysis results for different design approaches for stainless steel members with stocky cross-sections under combined loading.

Design approach	Stainless steel family	n	b	V_δ	V_r	γ_{M1}
Design Approach 0	Austenitic	198	1.232	0.079	0.111	0.94
	Ferritic	201	1.253	0.078	0.108	0.96
	Duplex	196	1.227	0.054	0.093	0.94
Design Approach 1	Austenitic	198	1.237	0.064	0.101	0.90
	Ferritic	201	1.183	0.073	0.104	1.00
	Duplex	196	1.200	0.045	0.088	0.94
Design Approach 2	Austenitic	198	1.184	0.058	0.097	0.93
	Ferritic	201	1.169	0.073	0.104	1.01
	Duplex	196	1.178	0.044	0.087	0.96
Design Approach 3	Austenitic	198	1.141	0.063	0.100	0.98
	Ferritic	201	1.154	0.079	0.108	1.04
	Duplex	196	1.145	0.049	0.090	1.00
Design Approach 4	Austenitic	198	1.130	0.065	0.101	0.99
	Ferritic	201	1.151	0.080	0.109	1.05
	Duplex	196	1.139	0.050	0.090	1.00

Table 12. Summary of the reliability analysis results for different design approaches for stainless steel members with slender cross-sections under combined loading.

Design approach	Stainless steel family	n	b	V_δ	V_r	γ_{M1}
Design Approach 0	Austenitic	92	1.310	0.126	0.148	1.05
	Ferritic	93	1.406	0.087	0.114	0.89
	Duplex	120	1.358	0.083	0.112	0.93
Design Approach A	Austenitic	92	1.295	0.112	0.136	1.02
	Ferritic	93	1.310	0.077	0.107	0.92
	Duplex	120	1.293	0.066	0.100	0.93
Design Approach B	Austenitic	92	1.265	0.100	0.127	1.00
	Ferritic	93	1.301	0.080	0.109	0.95
	Duplex	120	1.273	0.062	0.098	0.94
Design Approach C	Austenitic	92	1.284	0.108	0.133	1.02
	Ferritic	93	1.296	0.076	0.106	0.93
	Duplex	120	1.268	0.067	0.101	0.95
Design Approach D	Austenitic	92	1.251	0.096	0.123	1.00
	Ferritic	93	1.283	0.079	0.108	0.96
	Duplex	120	1.246	0.066	0.100	0.97

Table 13. Summary of the reliability analysis results for different design approaches for stainless steel members under combined loading (including stocky and slender cross-sections).

Design approach	Stainless steel family	n	b	V_δ	V_r	γ_{M1}
Design Approach 0	Austenitic	290	1.256	0.099	0.126	1.00
	Ferritic	294	1.286	0.093	0.119	0.98
	Duplex	316	1.278	0.082	0.112	0.98
Design Approaches 1 & A	Austenitic	290	1.255	0.084	0.114	0.96
	Ferritic	294	1.211	0.085	0.112	1.01
	Duplex	316	1.235	0.065	0.099	0.97
Design Approaches 3 & B	Austenitic	290	1.179	0.089	0.118	1.02
	Ferritic	294	1.186	0.094	0.119	1.07
	Duplex	316	1.194	0.075	0.106	1.03
Design Approaches 4 & D	Austenitic	290	1.168	0.089	0.118	1.03
	Ferritic	294	1.180	0.092	0.118	1.07
	Duplex	316	1.180	0.071	0.104	1.03